

February 1966



USCEE Report 161

UNIVERSITY OF SOUTHERN CALIFORNIA

SCHOOL OF ENGINEERING

FINAL REPORT

MILLIMETER-WAVE RADIOMETRY FOR RADIO ASTRONOMY

W. V. T. Rusch

S. Slobin

C. T. Stelzried

Contract No. JPL 951 004

Prepared for
JET PROPULSION LABORATORY
PASADENA, CALIFORNIA

ELECTRONICS SCIENCES LABORATORY

GPO PRICE \$

CFSTI PRICE(S) \$

Hard copy (HC)

Microfiche (MF)

~~\$~~ 3.00

1.75

ff 653 July 65

(TITLE)

(CODE)

(CATEGORY)

43

1100

February 1966

USCEE Report 161

MILLIMETER -WAVE RADIOMETRY FOR RADIO ASTRONOMY

W. V. T. Rusch

S. Slobin

C. T. Stelzried

FINAL REPORT

Contract No. JPL 951 004

Prepared for
JET PROPULSION LABORATORY
PASADENA, CALIFORNIA

**This work was performed for the Jet Propulsion Laboratory,
California Institute of Technology, sponsored by the
National Aeronautics and Space Administration under
Contract NAS7-100.**

TABLE OF CONTENTS

I. HISTORY OF THE PROGRAM	1
II. INSTRUMENTATION DEVELOPMENT	3
A. IF-Amplifier Development.	3
B. Calibrated Thermal Terminations	6
C. Local Oscillator	6
D. Digital Recorder	6
E. Reflectometer	7
III. ANTENNA DEVELOPMENT	8
A. Antenna Drive Modifications	8
B. Polar Mount	8
C. Mirror Coating	9
D. Antenna Pattern Measurements	9
E. Antenna Gain Measurements	9
F. Nodding Subdish	15
IV. LUNAR ECLIPSE OF 19 DECEMBER 1964	20
A. Observational Data	23
1. 17 December 1964	23
2. 19 December 1964 (12 Midnight - 3:54 AM PST)	27
3. 19 December 1964 (6:28 - 8:13 PM PST).	28
4. 18 December 1964	
B. Calculated Insolation Curve During Lunar Eclipse of 19 December 1964	33
C. One-Dimensional Heat-Flow Computer Program	33
D. Theoretical Radiometric Eclipse Curves for the Lunar Eclipse of 19 December 1964	37
V. LUNATION OBSERVATIONS	41
A. Observations	41
B. Data Reduction	47
ACKNOWLEDGEMENT	59

I. HISTORY OF THE PROGRAM

In September, 1963, the mm-wave instrumentation program was initiated as a joint effort between the Jet Propulsion Laboratory and the Electrical Engineering Department of the University of Southern California. The JPL participation was conducted through the New Circuit Elements Group of the Communications Elements Research Section, which provided equipment and personnel involved primarily with the electronic instrumentation.

The Electrical Engineering Department contributed the antenna, a converted 60-inch searchlight. Personnel were provided to design the antenna and feed system, the associated drive system, etc. USC personnel also directed the astronomical aspects of observation of the lunar eclipse of 30 December 1963. During the period from September 1963 to July 1964 USC participation was sponsored by a grant from the Research Corporation, Contract AJ4-205 638 from JPL, and financial support for salaries and equipment from the EE Department, Joint Services Grant, AF-AFOSR-496-64.

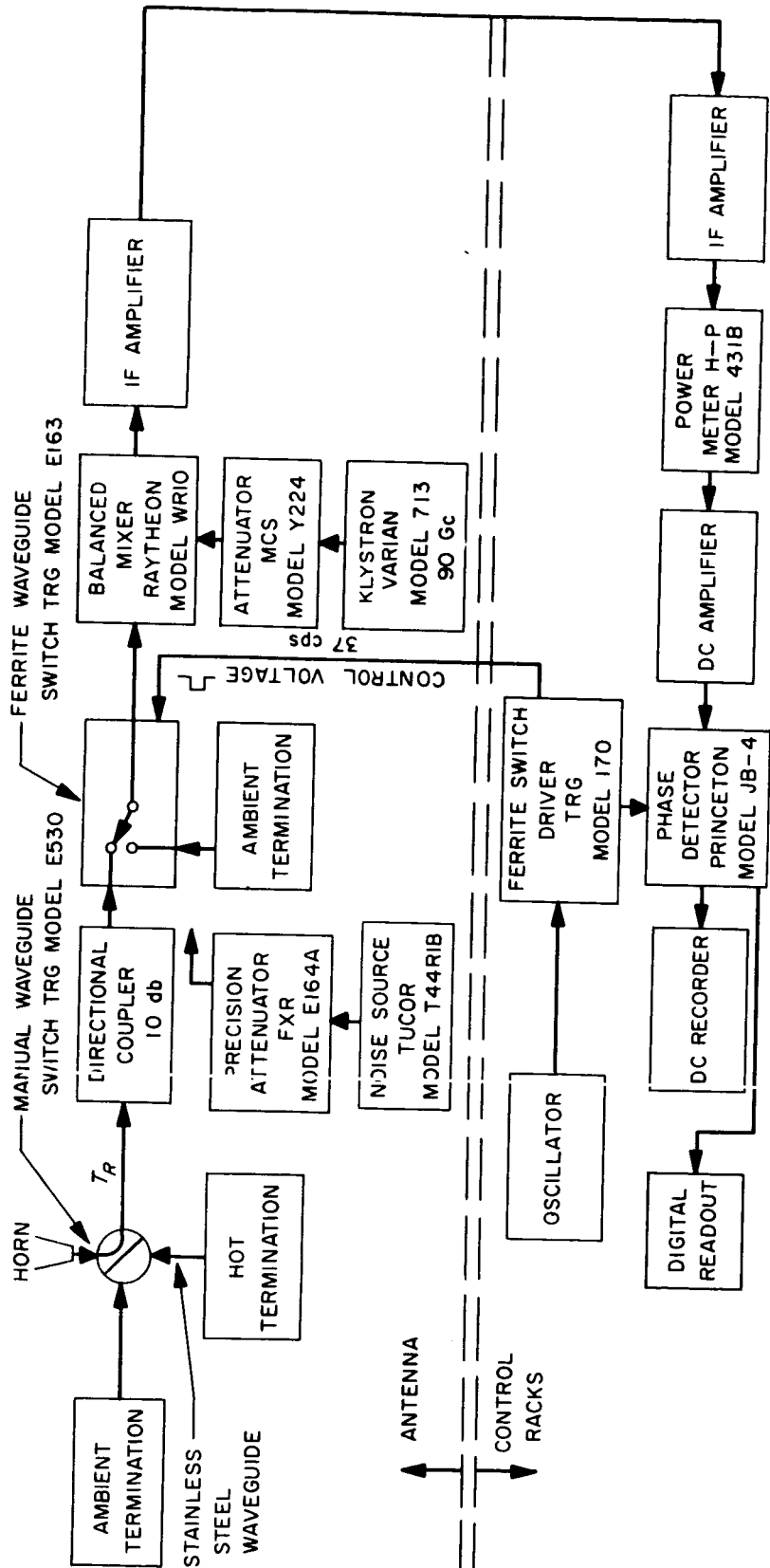
In August, 1964 a JPL study contract was issued to the USC Electrical Engineering Department (JPL Contract No. 951 004). The purpose of this contract was to investigate and develop high sensitivity MM-wave receivers and the techniques of their application to scientific and technological experimentation. The original contract period was from 1 August 1964 to 31 July 1965; however, a two-month extension changed the termination date to 30 September 1965. This contract continued the previous work as a joint

JPL-USC program. The mm-wave radiometer and associated electronic technologies were the primary areas of interest and responsibility of JPL, although there was considerable participation by USC personnel in the design and assembly stages of the radiometer, particularly during the summer months. The chief responsibilities of the USC personnel were antenna design and performance, the scientific observational program, the theoretical analyses, and data reduction. The overall long-range planning of the entire program was a mutual effort.

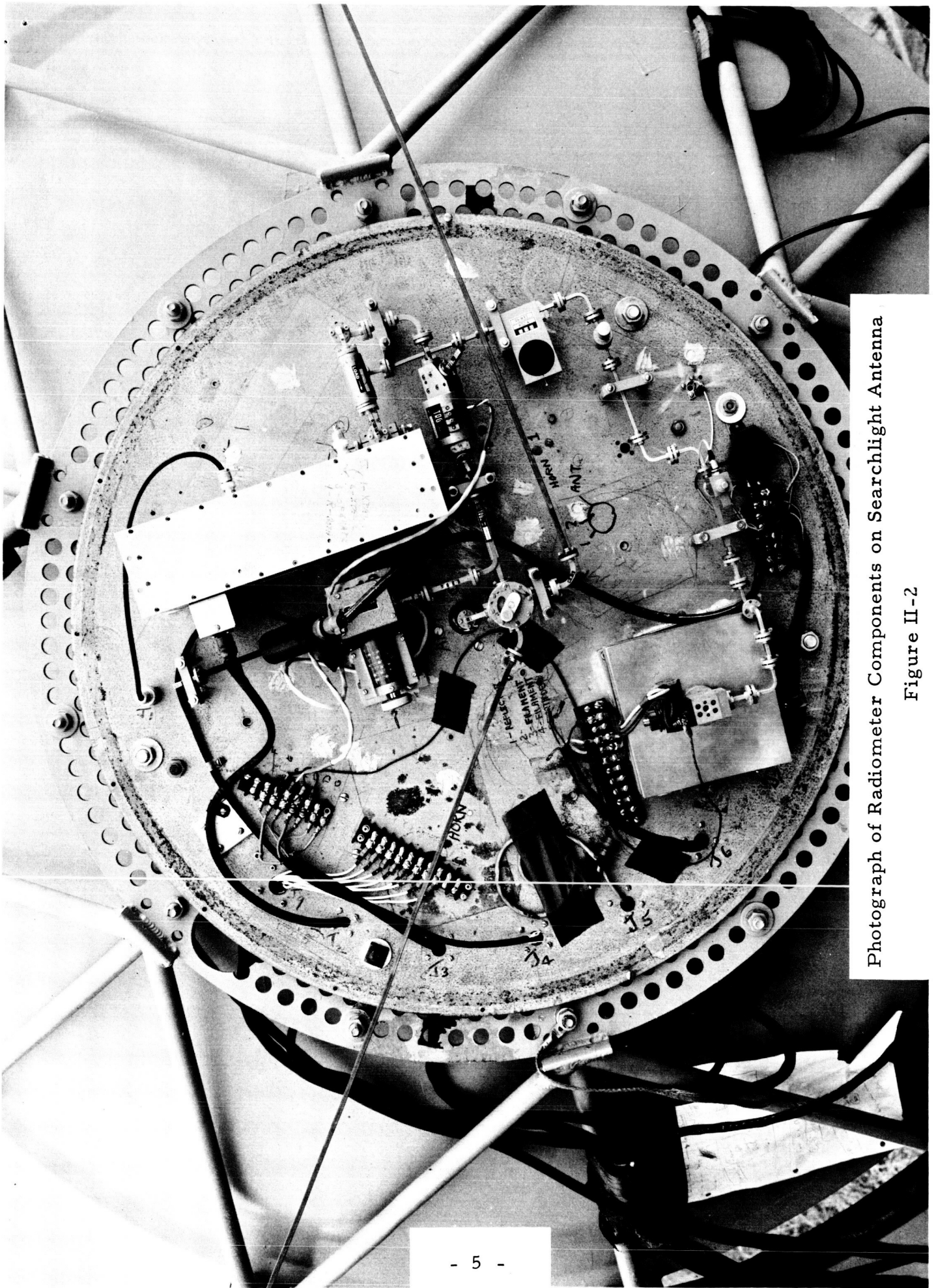
II. INSTRUMENTATION DEVELOPMENT

Inasmuch as instrumentation development was primarily a JPL responsibility, major progress in this area was generally reported in detail in JPL Space Programs Summaries Nos. 37-29, 37-30, 37-31, 37-32, 37-33, 37-34, and 37-35, Volume IV. However, where pertinent for continuity, important instrumentation developments during the term of this contract are included briefly in this report. The instrumentation centers around the 90-Gc (3.3 mm) Dicke-type superheterodyne radiometer. The radiometer block diagram is shown in Fig. II-1 and a photograph of the RF components on the antenna is shown in Fig. II-2.

A. IF-Amplifier Development. In the Spring of 1965 a wide-band (65-Mc bandwidth) commercial transistorized IF amplifier (Hewlett-Packard Model 461A) replaced the original 10-Mc. IF amplifier in the radiometer, resulting in considerably improved sensitivity (Cf. Figs. IV-3 and V-1). The amplifier was repackaged in a welded aluminum box to eliminate IF leakage. 115 volt ac line filtering was provided. A wide-band transformer was modified to match the push-pull output of the radiometer balanced mixer to a single-ended amplifier input. A 2N3783 low-noise transistor was incorporated into the first stage; the resulting noise figure was 3.2 db at 50 Mc working into a 200-ohm single-ended input impedance. The equivalent noise temperature of the radiometer (at 90 Gc) was measured to be approximately 20,000 degrees K, and the associated peak-to-peak noise jitter (measured) is 6 degrees Kelvin (for a one-second post-detection time constant).



Block Diagram of 90-Gc Radiometer
Figure II-1



Photograph of Radiometer Components on Searchlight Antenna

Figure II-2

B. Calibrated Thermal Terminations. Precision RG-99/U waveguide calibrated thermal terminations have been constructed. These terminations consist of a well-matched waveguide load, soft-soldered inside a solid copper cylinder which is about two inches long and one inch in diameter. The copper cylinder is snugly mounted inside an anodized aluminum heat sink around which is wound nichrome heater wire. A stainless steel waveguide section leading to the load is gold plated with an electrodeless plating technique. These loads are used for an accurate thermal calibration of the radiometer.

C. Local Oscillator. The Raytheon klystron (QKK 1152) was replaced by a well heat-sunk Varian klystron (VC 710B) as the 90-Gc local oscillator. This new klystron resulted in a significant improvement in both long-term stability and noise jitter of the radiometer. The LO amplitude output was measured to have a short-term amplitude jitter of about 0.01 db and a long-term drift of less than 0.05 db over a span of several hours. The short-term frequency jitter is about 0.5 Mc. The excellent stability of the Varian klystron facilitated measurement of the RF response of the radiometer, and measurement of antenna gain and pattern.

D. Digital Recorder. A digital output system consisting of a Dymec Integrating Voltmeter 2401A driving a Hewlett Packard Digital Recorder 562A has been incorporated into the radiometer in parallel with the analog output (strip-chart recorder). This digital system greatly facilitates the accuracy and convenience of data reduction.

E. Reflectometer. A 90-Gc reflectometer has been assembled using a TRG, Inc. circulator. VSWR's as small as 1.01:1 can be measured with this reflectometer, whereas the residual VSWR of the FXR, Inc. slotted line is about 1.03:1.

III. ANTENNA DEVELOPMENT

A 60-inch searchlight, modified by the USC Electrical Engineering Department under JPL contract No. AJ4-205 638, was used as a small, Cassegrainian-fed mm-wave antenna in conjunction with the radiometric instrumentation developed under this contract. Although easily transportable, the searchlight was mounted on a concrete pad at a semi-permanent site on the JPL Mesa Antenna Range in Pasadena. A nearby Contraves phototheodolite installation was available to support the mm-wave experiments.

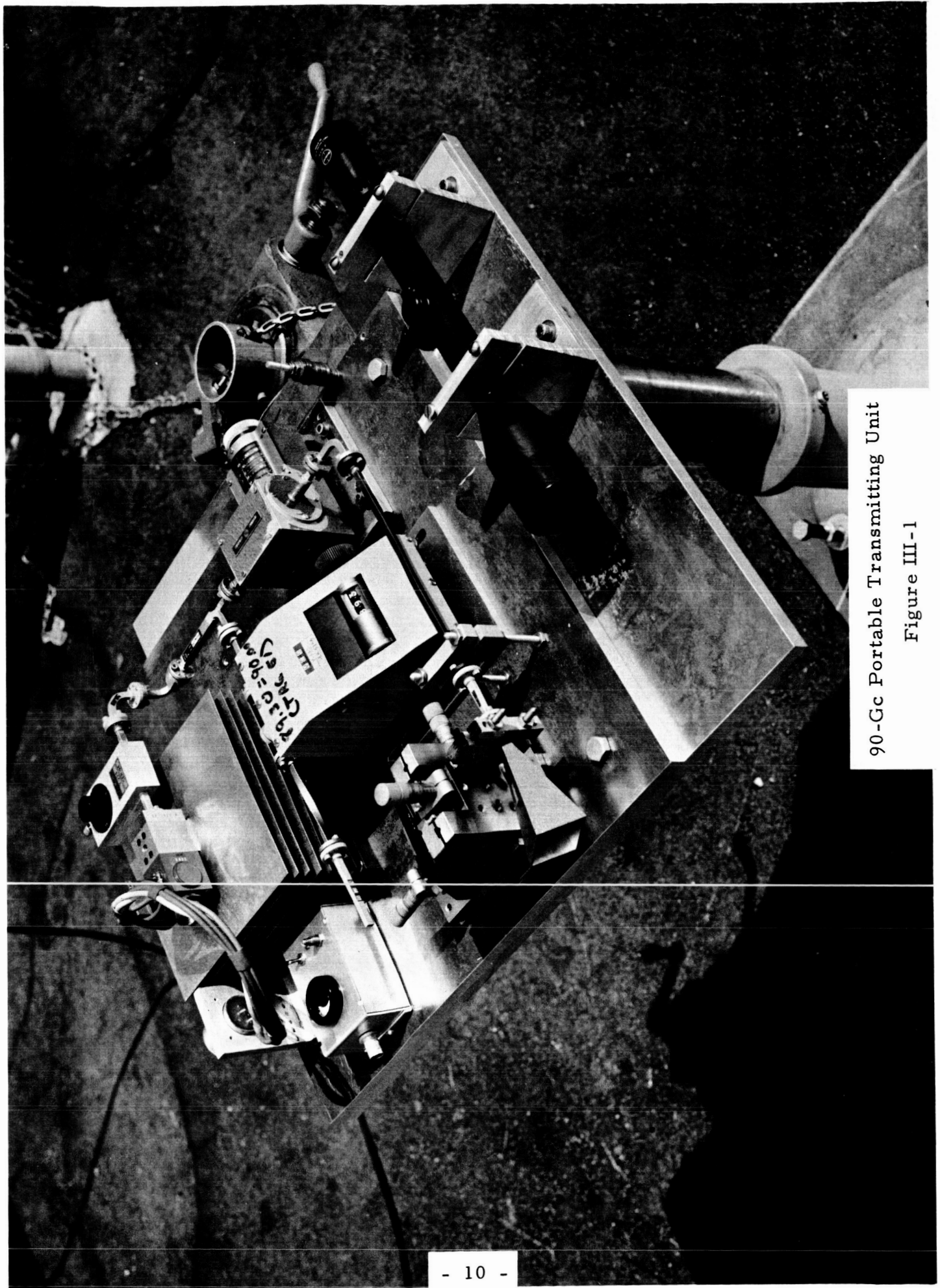
A. Antenna Drive Modifications. Special couplings to the Slosyn motors were installed. These couplings have sufficient torsional deflections to reduce the peak acceleration transmitted to the antenna axles but not enough to affect the positioning controls. These couplings proved to be only moderately successful, since a small amount of "jerk" remains in the drive, particularly during slewing. Consequently use of the slewing controls was kept to a minimum. However, the electric stepping controls were used with good results during antenna pattern measurements, and the sidereal tracking drive was used, also with considerable success, for tracking celestial objects.

B. Polar Mount. A motor-driven unit for tilting the antenna into a polar position was designed, fabricated, and installed. This unit consists of a 58-inch lead screw, coupled by means of a worm and worm-gear to a Bodine #B4208-40 electric motor. Presently the antenna can be polar-mounted at any site north of approximately 33 degrees N. latitude.

C. Mirror Coating. A coating of high-reflectance white semi-gloss vinyl paint over a thin coat of zinc-chromate primer was applied to the rhodium-plated copper mirror. This coating virtually eliminated concentration of short-wavelength radiation at the antenna focus. Solar observations can thus be made without excessive overheating. However, preliminary sky-temperature measurements indicate that this coating may have degraded the overall antenna gain by as much as 0.25 - 0.30 db.

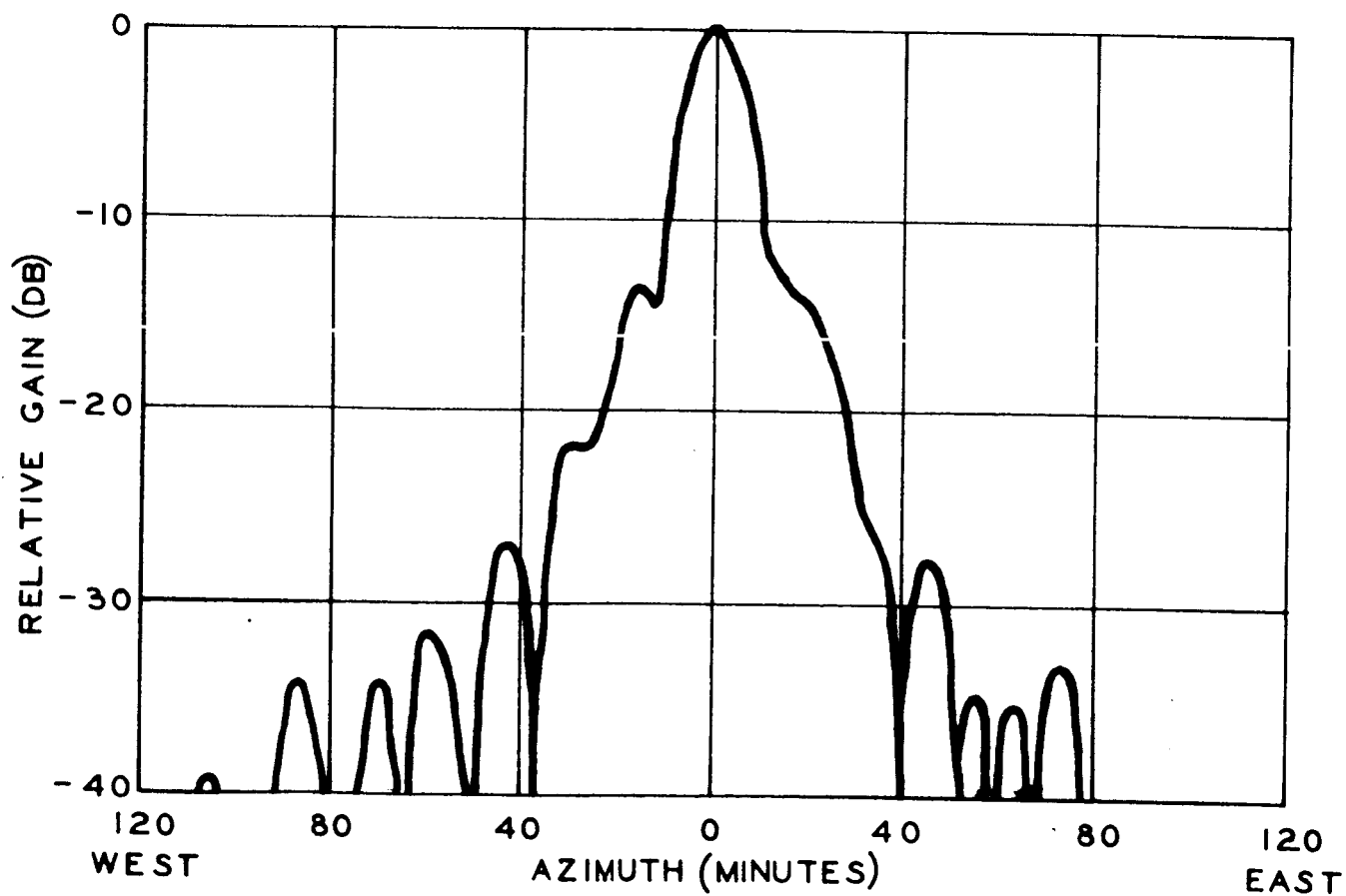
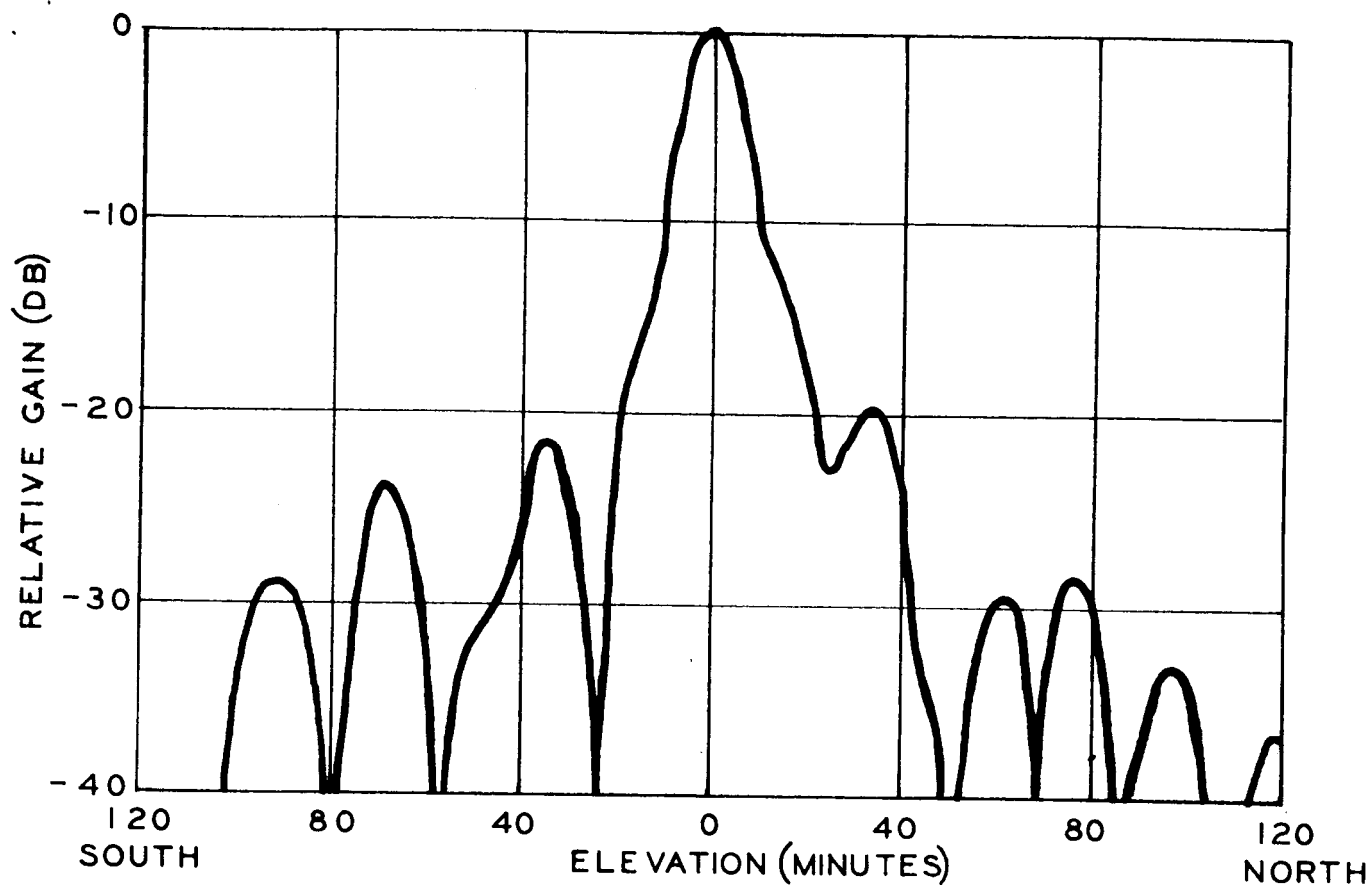
D. Antenna Pattern Measurement. A portable transmitting unit (Fig. III-1) was installed at a distance of approximately 3500 feet ($1.5 D^2 / \lambda$) from the searchlight antenna. The intervening terrain fell rapidly away into a deep valley. The power density from the transmitter was sufficiently great at the antenna that a dynamic range of 40 db was available for preliminary antenna pattern measurements. The resulting elevation and azimuth patterns are plotted in Fig. III-2. The measured 10.5-minute half-power beamwidth was greater than the theoretically predicted beamwidth (9 minutes), indicating the need for an improved feed-system design. The antenna patterns were integrated to obtain necessary beam-correction factors (BCF) for reduction of lunar observation data. The gain and beamwidth were remeasured at a distance of approximately $5 D^2 / \lambda$ with no appreciable change.

E. Antenna Gain Measurements. The transmitting setup described in (D) was used to measure the peak antenna gain (including all losses between the aperture of the antenna and the output of the waveguide switch). Two identical standard gain horns were mounted on opposite sides of the mouth of the 60-inch



90-Gc Portable Transmitting Unit

Figure III-1



Measured Antenna Patterns of 90-Gc Searchlight Antenna
Figure III-2

searchlight antenna. These horns were connected to the waveguide switch by means of long waveguide runs of known insertion loss. The gain setup is pictured in Fig. III-3 where:

G_1 = 90-Gc gain of reference horn #1 at mouth of horn = 25.22 db
(theoretical)

G_2 = 90-Gc gain of reference horn #2 at mouth of horn = 25.22 db
(theoretical)

G_A = 90-Gc gain of 60-inch searchlight antenna in plane of aperture

L_{H1} = loss between mouth and output flange of horn #1 (unknown, assumed small)

L_{H2} = loss between mouth and output flange of horn #2 (unknown, assumed small)

L_A = loss between mouth of 60-inch antenna and mouth of feed horn, including possible absorption in antenna paint

L_1 = loss in long waveguide run from horn #1 to waveguide switch = 6.78 db (measured)

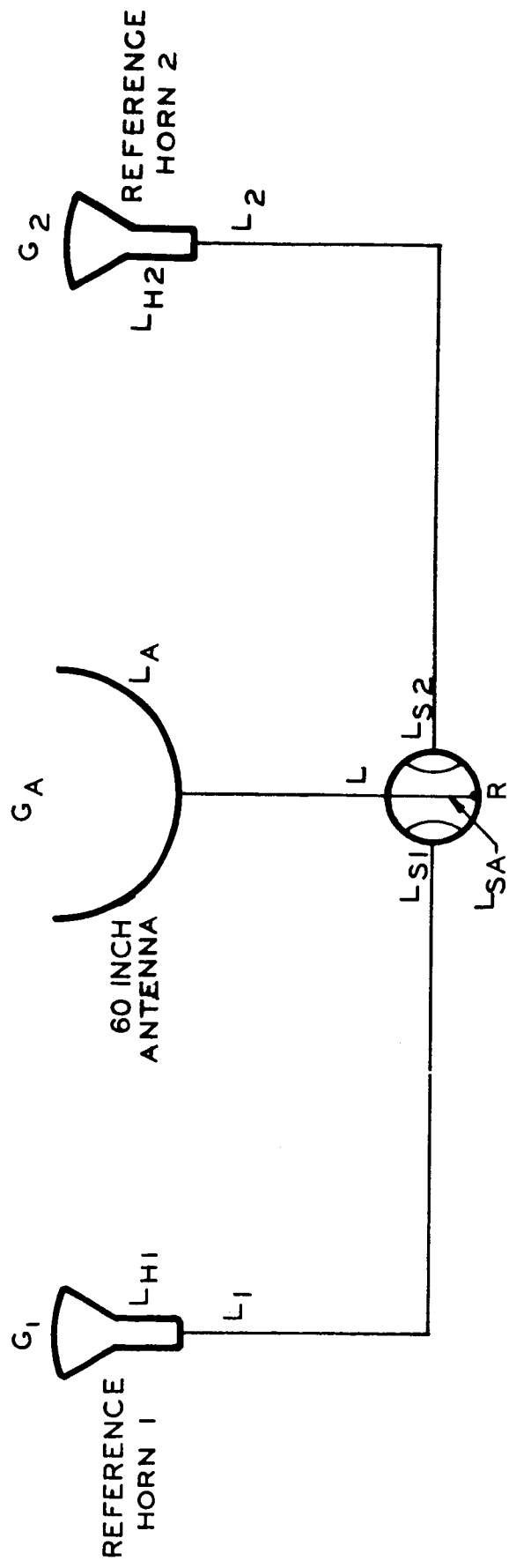
L_2 = loss in long waveguide run from horn #2 to waveguide switch = 6.87 db (measured)

L = loss in feed-horn and E-plane bend to waveguide switch

L_{S1} = loss in switch path from R (reference point) toward horn #1 = .33 db
(measured)

L_{S2} = loss in switch path from R toward horn #2 = .38 db (measured)

L_{SA} = loss in switch path from R toward antenna ($L + L_{SA} \leq 0.5$ db)



Schematic Diagram of Setup to Measure Antenna Gain

Figure III - 3

The calibration scheme proceeded as follows:

1. The main beams of the antenna and the reference horns were directed at the transmitter and the polarizations were properly aligned. The transmitter was adjusted to produce a power density P_{TO} at the receiving site.

2. With the waveguide switch in the antenna-position P_R , the power received by the antenna at R, was

$$P_R = P_{TO} + G_A - (L_A + L + L_{SA}) \quad (\text{III-1})$$

3. With the waveguide switch in the reference horn #1-position, the transmitted power is increased by a factor F_1 (db) with the calibrated attenuator at the transmitter site so that the power received by horn #1 at R was also P_R .

Then:

$$P_R = P_{TO} + F_1 + G_1 - (L_{H1} + L_1 + L_{S1}) \quad (\text{III-2})$$

Equating (III-1) and (III-2) yields:

$$G_A - (L_A + L + L_{SA}) = F_1 + G_1 - (L_{H1} + L_1 + L_{S1}) \quad (\text{III-3})$$

4. This procedure can be repeated using reference horn #2; then

$$G_A - (L_A + L + L_{SA}) = F_2 + G_2 - (L_{H1} + L_1 + L_{S1}) \quad (\text{III-4})$$

Repeating (III-3) and (III-4) many times to reduce the effect of random experimental uncertainty yielded

$$G_A - (L_A + L + L_{SA}) = 56.92 \text{ db} \pm .25 \text{ db} \quad (\text{III-5})$$

The estimated uncertainty is attributed primarily to measurement error. The corresponding value of power gain ratio is 4.92×10^5 , and the equivalent 60-inch aperture efficiency at 90 Gc is 0.24 (at the output of the waveguide switch).

Two major causes of error were discovered in the gain and pattern measurements. Because of the highly sensitive receiver and the wide dynamic range covered in the measurement, RF leakage at the transmitter can cause rapid fluctuations of the received signal. These fluctuations, which can be many db in magnitude, are eliminated by carefully shielding the RF path between the klystron and the calibrated attenuator at the transmitter. The received signal must drop to zero when the transmitter horn is completely shorted.

In addition the "calibrated" attenuators are disproportionately inaccurate at high values of attenuation. More accuracy is obtained by combining two or more in series so that each attenuator need be set at a relatively low value.

F. Nodding Subdish. Synchronous switching techniques are generally used to detect weak radio-astronomical signals in the presence of relatively high noise contributions from the atmosphere and the receiver itself. One successful switching technique that has been used in radio astronomy has been to switch the antenna beam from the source to a nearby position in the sky. It appears possible that this beam-switching may be accomplished by periodically nodding the hyperboloidal subdish in the Cassegrainian feed system between two symmetrical but slightly off-axis positions.

A first-order analysis of a tilted subdish was carried out using simple reflection formulas from geometrical optics. The analysis clearly indicated

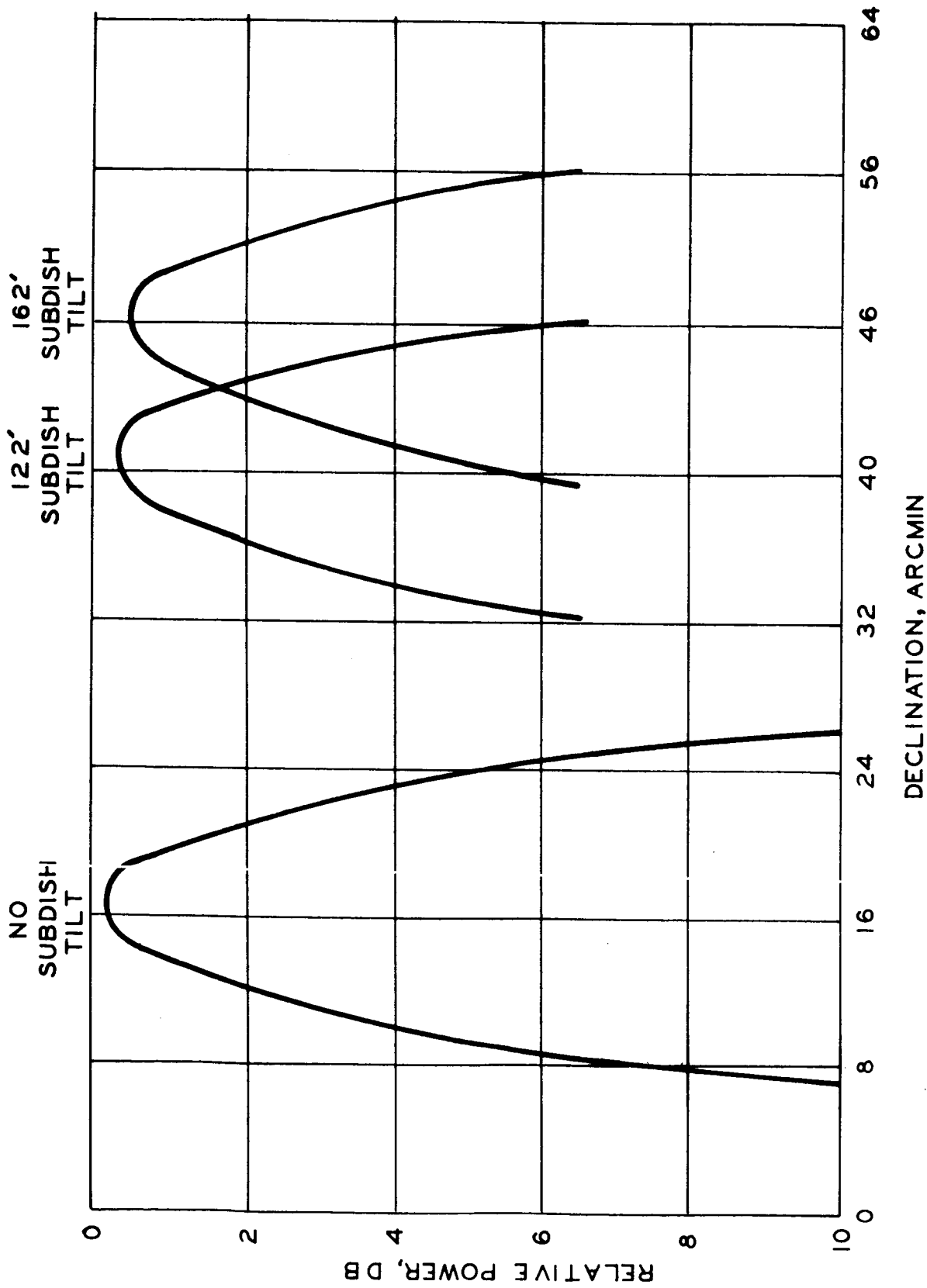
that the tilted hyperboloid does not have a point focus, but for small tilt angles the focal region remains sufficiently small so that an "average" focal point can be computed. As a result, however, some amount of aberration can be expected.

On 22 October 1964 a series of static pattern measurements was carried out. The pattern of an axially symmetric subdish is shown in Fig. III-4. The half-power beamwidth is approximately 10.5 minutes. The subdish was tilted to angles of 122 minutes and 162 minutes. The resulting patterns are indicated in Fig. III-4. Although a certain amount of gain degradation was evident, the pattern shape was not seriously deteriorated for the tilted subdish. The ratio of main-beam tilt to subdish tilt is about 1:5 (for the small range of angles considered). Comparison with the approximate ray-optics results indicates agreement for the main-beam tilt within 10%.

The mechanical design of the nodding subdish was completed. In this design the subdish and its counterweight are driven by a cam flywheel.

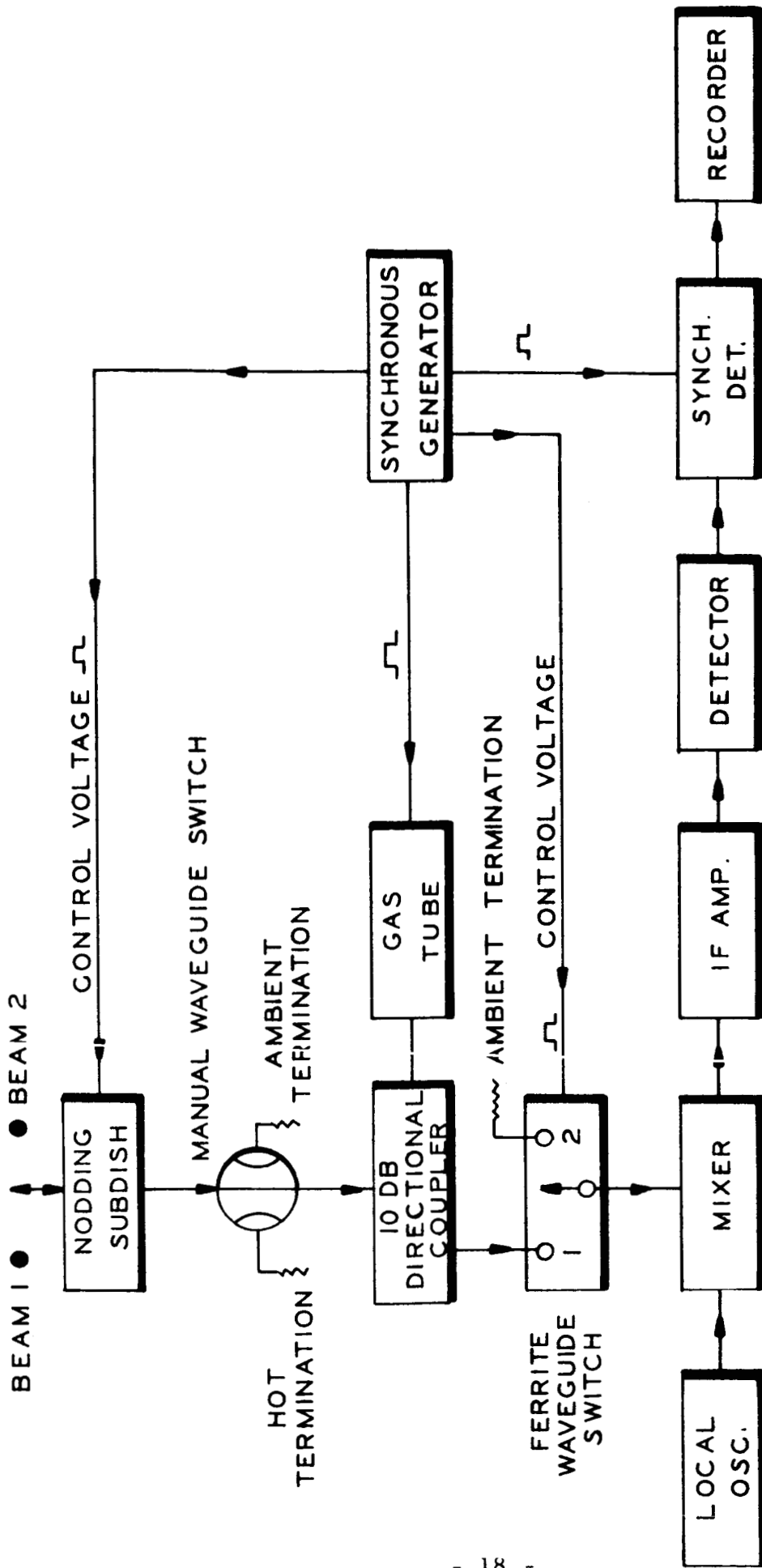
A major problem encountered in connection with the nodding-subdish scheme is the problem of thermal calibration. One contemplated calibration technique is schematically illustrated in Fig. III-5 and outlined below:

1. Waveguide switch turned to ambient load and ferrite circulator switched synchronously: $\text{output} = T_0 - T_0 = 0$
2. Waveguide switch turned to hot load and ferrite circulator switched synchronously: $\text{output} = T_H - T_0$
3. Waveguide switch turned again to ambient load; gas tube fired synchronously: $\text{output} = (T_0 + T_{GT}) - T_0 = T_{GT}$



E PLANE PATTERN OF MAIN ANTENNA BEAM FOR VARIOUS SUBDISH TILTS

Figure III-4



Block Diagram of Nodding Subdish Calibration System

Figure III-5

From (1) and (2) a scale factor is obtained in degrees Kelvin per unit output which is used to determine the equivalent noise temperature of T_{GT} in degrees Kelvin.

The data-taking technique associated with the above calibration technique proceeds as follows:

1. Replace ferrite switch with straight waveguide section.

2. Aim away from source and nod subdish synchronously: output =

$$T_{SKY} - T_{SKY} = 0$$

3. Continue aiming away from source; nod subdish synchronously;

gas tube fired synchronously when subdish is in position 1: output =

$$(T_{SKY} + T_{GT}) - T_{SKY} = T_{GT}$$

4. Turn off gas tube; aim one switching lobe at source, one switching

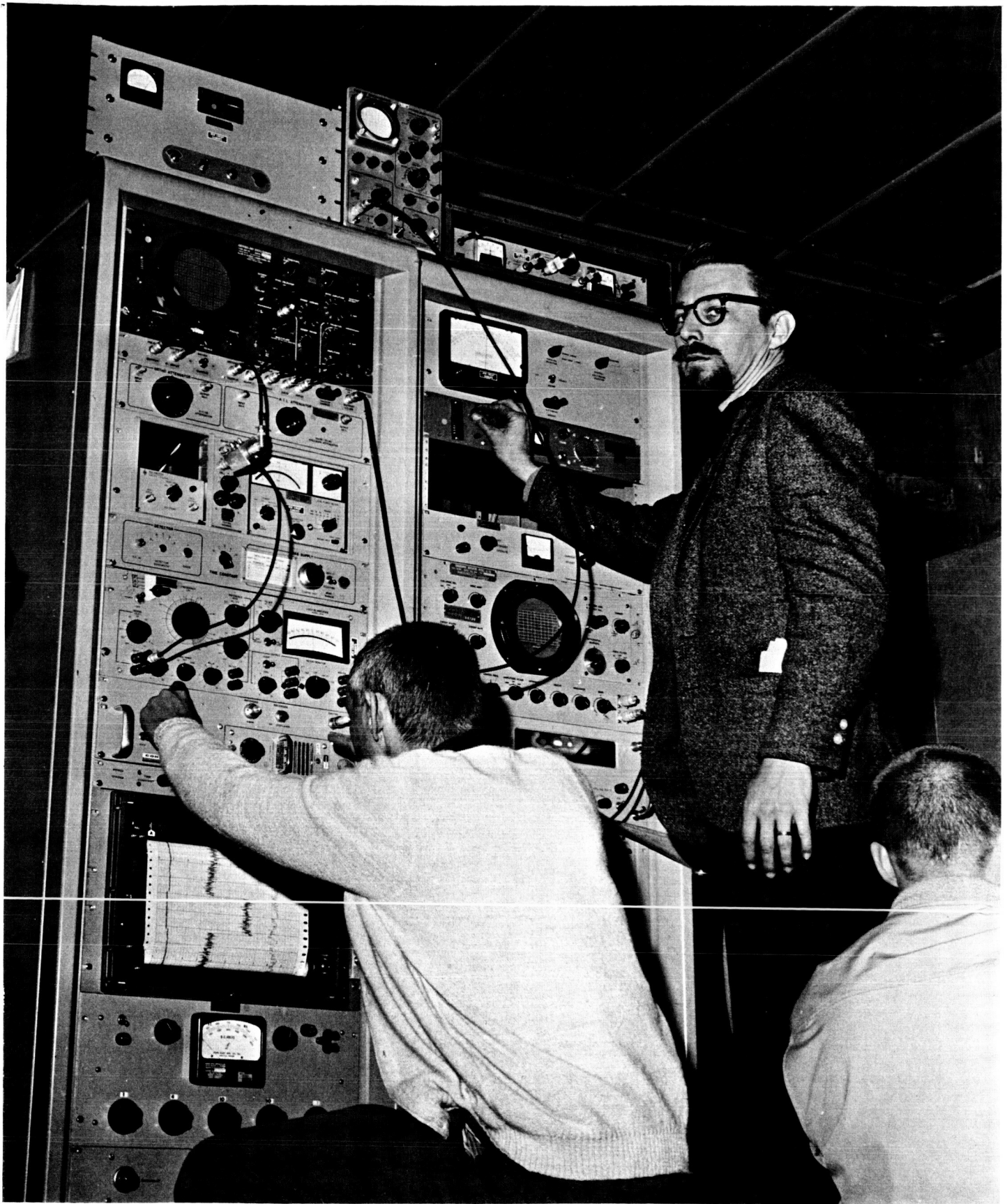
lobe at sky: output = $(T_{SOURCE} + T_{SKY}) - T_{SKY} = T_{SOURCE}$

IV. LUNAR ECLIPSE OF 19 DECEMBER 1964

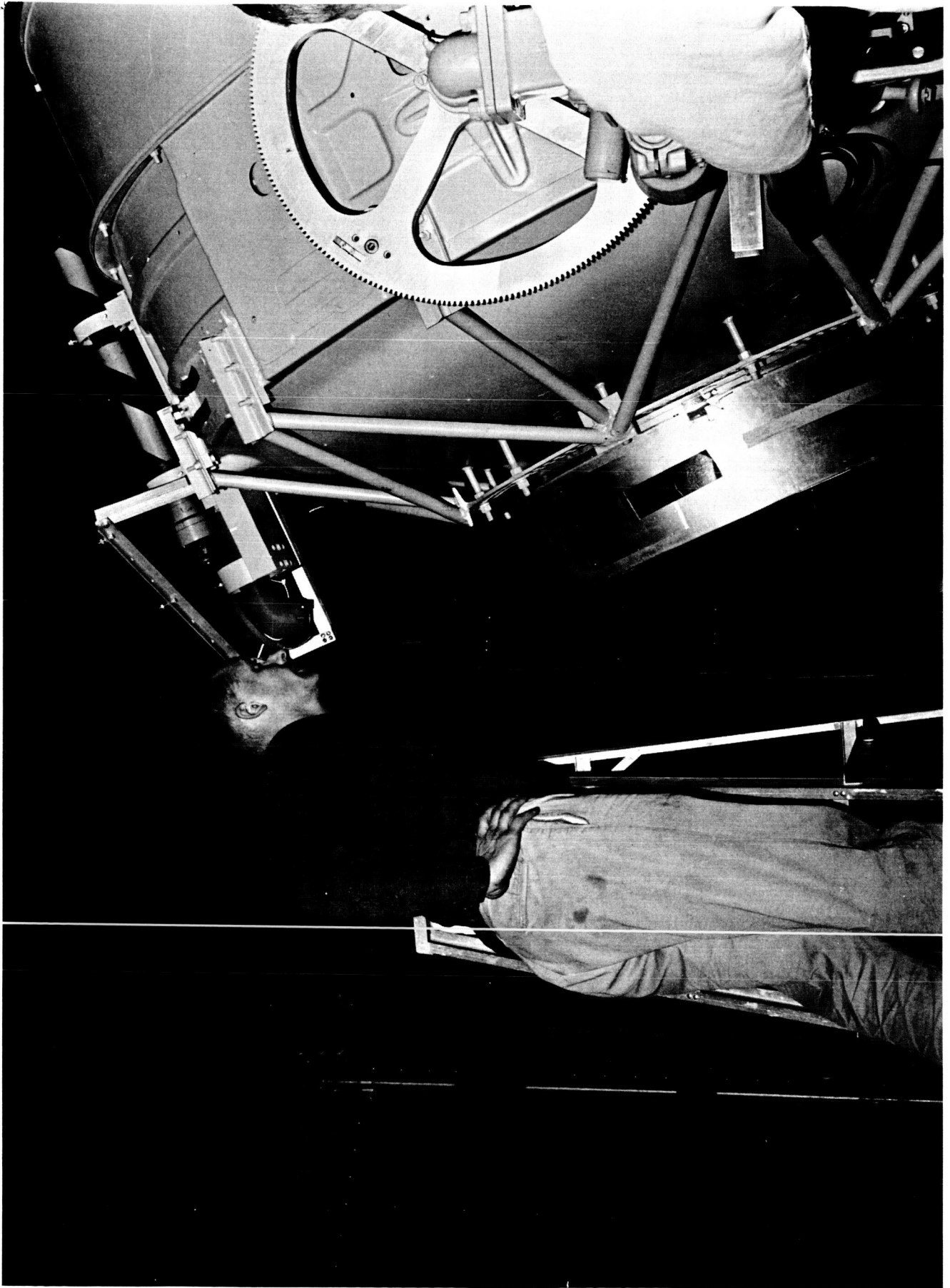
Preparations were made to observe the lunar eclipse from the existing site on the JPL Mesa Antenna Range. On 17 December, with the antenna in its final polar position, a series of lunar observations was carried out as a "dry-run" for the eclipse.

At daybreak on 18 December the weather in the Los Angeles area was overcast with intermittent rain. More rain was predicted for evening. Observations cannot be carried out in cloudy weather with the 90-Gc radiotelescope since optical tracking is used. Consequently, at 10:30 AM (PST) it was decided to transport the antenna, the two racks of electronic instrumentation, and boxes of associated hardware and tools to Palm Springs, one of two locations in Southern California with clear skies predicted for that evening. A temporary site was provided by the Canyon Country Club in Palm Springs. The equipment left JPL at 2:45 PM via moving van and arrived in Palm Springs at approximately 5:30 PM. Fig. IV-1 shows the electronic instrumentation in the van, and Fig. IV-2 shows the antenna tracking procedure. The eclipse had begun before the equipment was operational at the new site; the first drift curve of the moon (7:10 PM PST) was taken at the end of totality. Eleven drift curves with analog and digital output were made before the end of the umbral phase and a total of 71 drift-curves were made during the night 18 December - 19 December (PST).

Each drift-curve sequence, which took approximately $6\frac{1}{2}$ minutes, consisted of:



Radiometer Instrumentation at Palm Springs Site
Figure IV-1



Tracking Procedure During Lunar Eclipse of 19 December 1964

Figure IV -2

1. Tracking the center of the moon for one minute.
2. Stopping the antenna and recording the time (obtained from a digital clock set by WWV) and the zenith angle of the center of the moon (measured with a transit).
3. Establishing a base line after the moon drifted out of the antenna beam.
4. Firing the gas tube for one minute to provide a calibration level.
5. Re-establishing a base-line after the gas tube had been turned off.

Figure IV-3 shows the analog and digital recordings for sequence #22 taken at 9:11 PM and a zenith angle of 36.3 deg. The postdetection time constant was 1 sec for the analog data and 10 sec for the digital data.

A series of 16 drift-curve sequences was carried out from the temporary Palm Springs site in the early evening of 19 December 1964, the night after the eclipse.

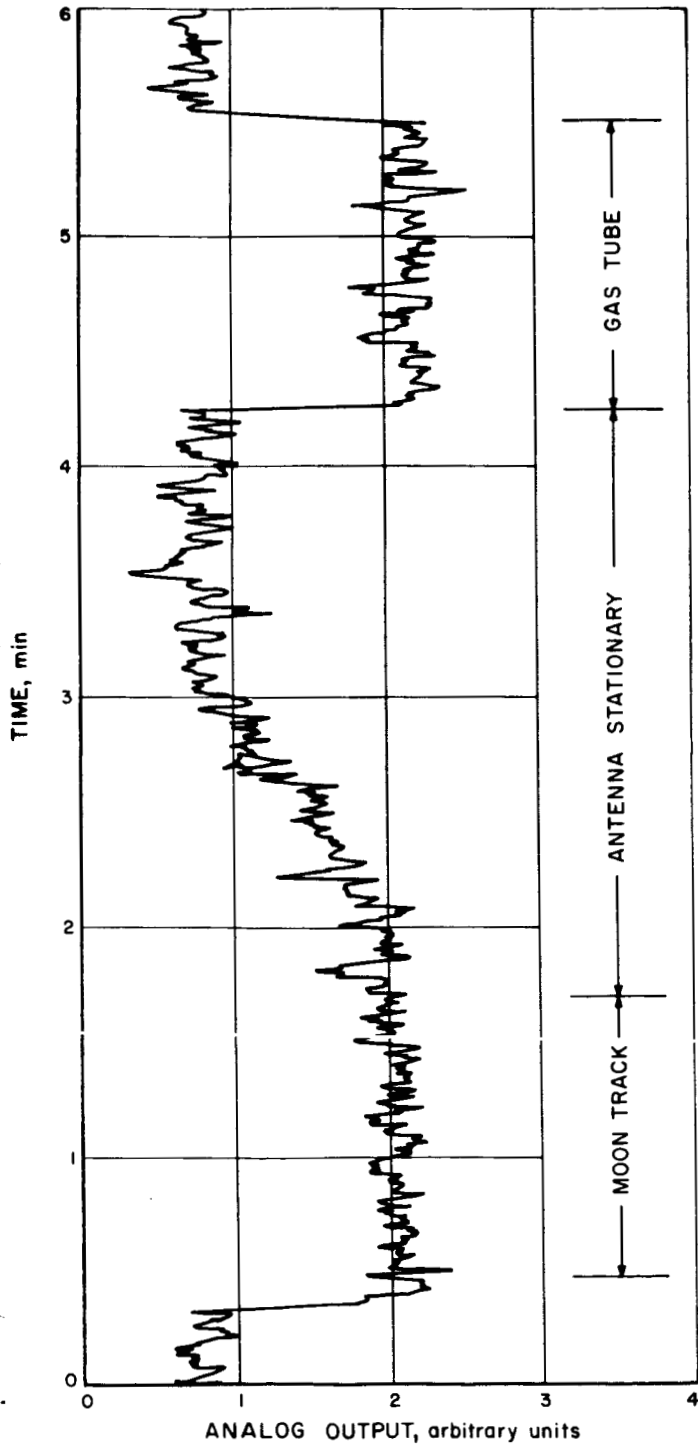
A. Observational Data.

1. 17 December 1964

29 drift curves of the moon were made on 17 December 1964 between 5:05 PM PST and 8:42 PM PST. The range of zenith angles was 75.1 to 31.9 deg. T'_M , the equivalent antenna temperature of the moon (without atmospheric absorption), is related to T' , the measured antenna temperatures, by

$$T' = T'_M(L_0)^{-AM(Z)} \quad (\text{IV-1})$$

where Z is the zenith angle, $AM(Z)$ is the equivalent "air mass" corresponding to each zenith angle, and L_0 is the atmospheric loss at $Z = 0$, i. e. unity "air



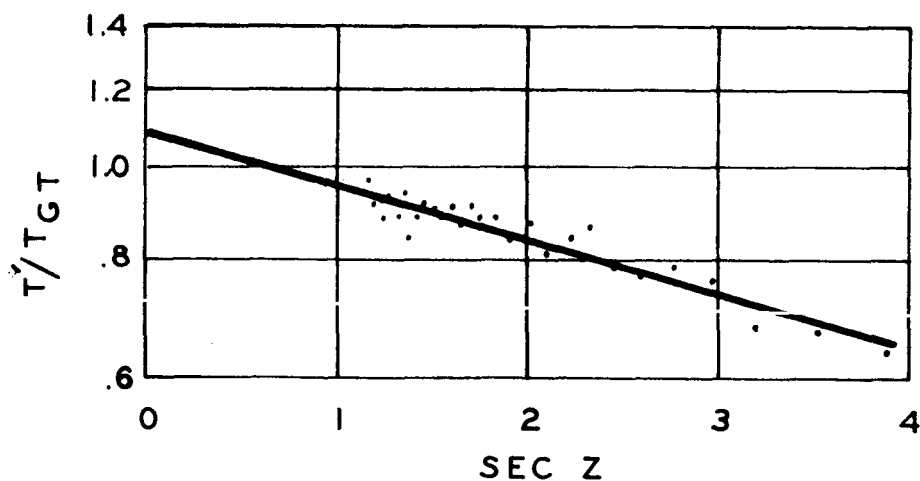
TIME			OUTPUT								
hr	min	sec	arbitrary units								
2	1	1	6	0	5	0	4	7	3	5	2
2	1	1	5	5	2	0	4	1	5	6	2
2	1	1	5	4	0	0	4	4	7	5	2
2	1	1	5	2	7	0	4	9	4	6	2
2	1	1	5	1	5	0	9	7	1	6	2
2	1	1	5	0	3	0	9	5	9	4	2
2	1	1	4	5	0	0	9	7	9	8	2
2	1	1	4	3	8	0	9	4	8	2	2
2	1	1	4	2	3	0	9	3	3	2	2
2	1	1	4	1	3	0	9	8	7	3	2
2	1	1	4	0	1	0	4	6	9	5	2
2	1	1	3	4	8	0	4	5	2	9	2
2	1	1	3	3	6	0	4	7	4	0	2
2	1	1	3	1	1	0	4	0	2	6	2
2	1	1	3	1	1	0	4	7	7	6	2
2	1	1	2	5	9	0	4	4	9	7	2
2	1	1	2	4	6	0	5	4	8	6	2
2	1	1	2	3	4	0	6	1	3	9	2
2	1	1	2	2	9	0	7	2	6	0	2
2	1	1	2	0	9	0	7	7	7	8	2
2	1	1	1	5	7	0	8	5	8	3	2
2	1	1	1	4	4	0	8	5	3	0	2
2	1	1	1	3	2	0	8	8	6	4	2
2	1	1	1	4	3	0	9	0	5	3	2
2	1	1	1	0	7	0	9	1	3	8	2
2	1	1	0	5	2	0	9	2	0	2	2
2	1	1	0	4	2	0	9	0	3	9	2
2	1	1	0	3	0	0	9	1	9	7	2
2	1	1	0	1	0	0	9	1	4	3	2
2	1	1	0	5	0	0	4	5	6	4	2
2	1	0	9	5	2	0	4	4	3	8	2
2	1	0	9	4	0	0	4	3	6	9	2

Analog and Digital Recordings for Drift Curve #22
18 December 1964

Figure IV-3

mass". Assuming that the primary contribution to the 90-Gc loss is due to water vapor, and the scale height of the water vapor in the atmosphere is 5 km, then $AM(Z)$ may be approximated by secant Z with less than 1% error up to angles of 80 deg; if the scale height is assumed to be 20 km, then the secant Z approximation results in a maximum error of 1.5% for Z less than 75 deg. Consequently $AM(Z)$ was replaced by secant Z in eq. (IV-1), which is equivalent to a flat-earth approximation.

Observational results from 17 December are plotted in Fig. IV-4:



17-December-1964 Lunar Data with "Best-fit" Straight Line Approximation;

$$T'_M/T_{GT} = 1.087 \pm .014 \text{ (p. e.)}; L_0 = 1.135 \pm .007 \text{ (p. e.)}$$

Figure IV-4

The logarithm of the ratio of the observed antenna temperature to the gas-tube equivalent excess noise temperature (at the output of the waveguide switch) is plotted versus $\sec Z$ for each data point. It is possible to fit these data points with the best straight line using a least-squares criterion. This is then the best-fit straight line to the equation

$$\log T' = \log T'_M - \sec Z \log L_0 \quad (\text{IV-2})$$

However, the linearization of eq. (IV-1) to yield (IV-2) implicitly introduces certain undesired weighting factors into the least-squares procedure. Consequently a Taylor series iteration method has been used to obtain the values of L_0 and T'_M which best fit eq. (IV-1) directly. [In general the values computed in this manner are only a few percent different from the linearization procedure used with eq. (IV-2).] For the 17-December data:

$$T'_M / T_{GT} = 1.087 \pm .013 \text{ (p. e.)}$$

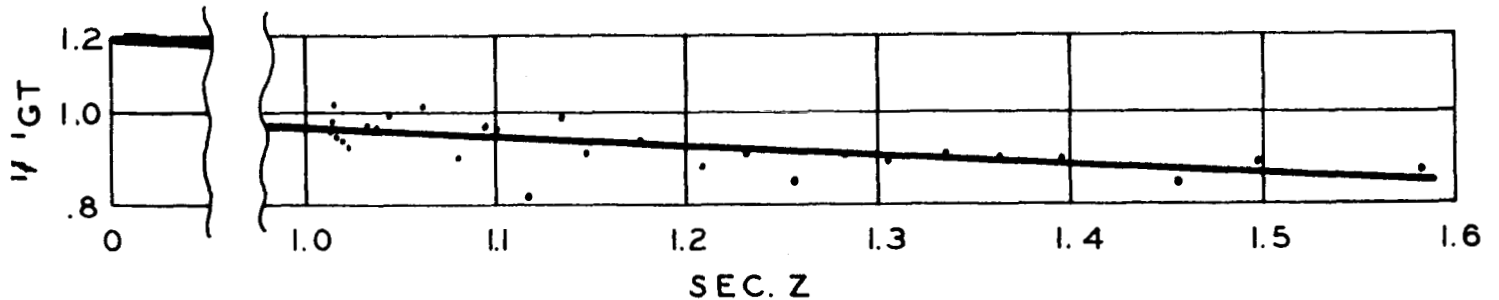
$$L_0 = 1.135 \pm .007 \text{ (p. e.)}$$

These values are used to generate the straight line shown with the data points in Fig. IV-4.

Thermal calibration of the gas-tube yielded $T_{GT} = 124.5^\circ \text{K}$ (at the output of the waveguide switch). Then $T'_M = 135.3^\circ \text{K}$. The antenna BCF appropriate to the lunar semi-diameter on 17 December (described in Section V) was 0.4911, yielding the equivalent blackbody disc temperature of the moon to be 275.5°K on 17 December.

2. 19 December 1964 (12 Midnight - 3:54 AM PST)

29 drift curves were made on 19 December 1964 between 0:00 AM PST and 3:54 AM PST. The range of zenith angles was 9.5 to 38.2 deg. The data are presented in Fig. IV-5:



19-December-1964 Lunar Data (0000 - 0400 HR PST) with "Best-fit"
Straight Line Approximation;

$$T'_M / T_{GT} = 1.197 \pm .048 \text{ (p. e.)}; L_0 = 1.248 \pm .042 \text{ (p. e.)}$$

Figure IV-5

Repeating the iteration procedure described in the previous section yielded

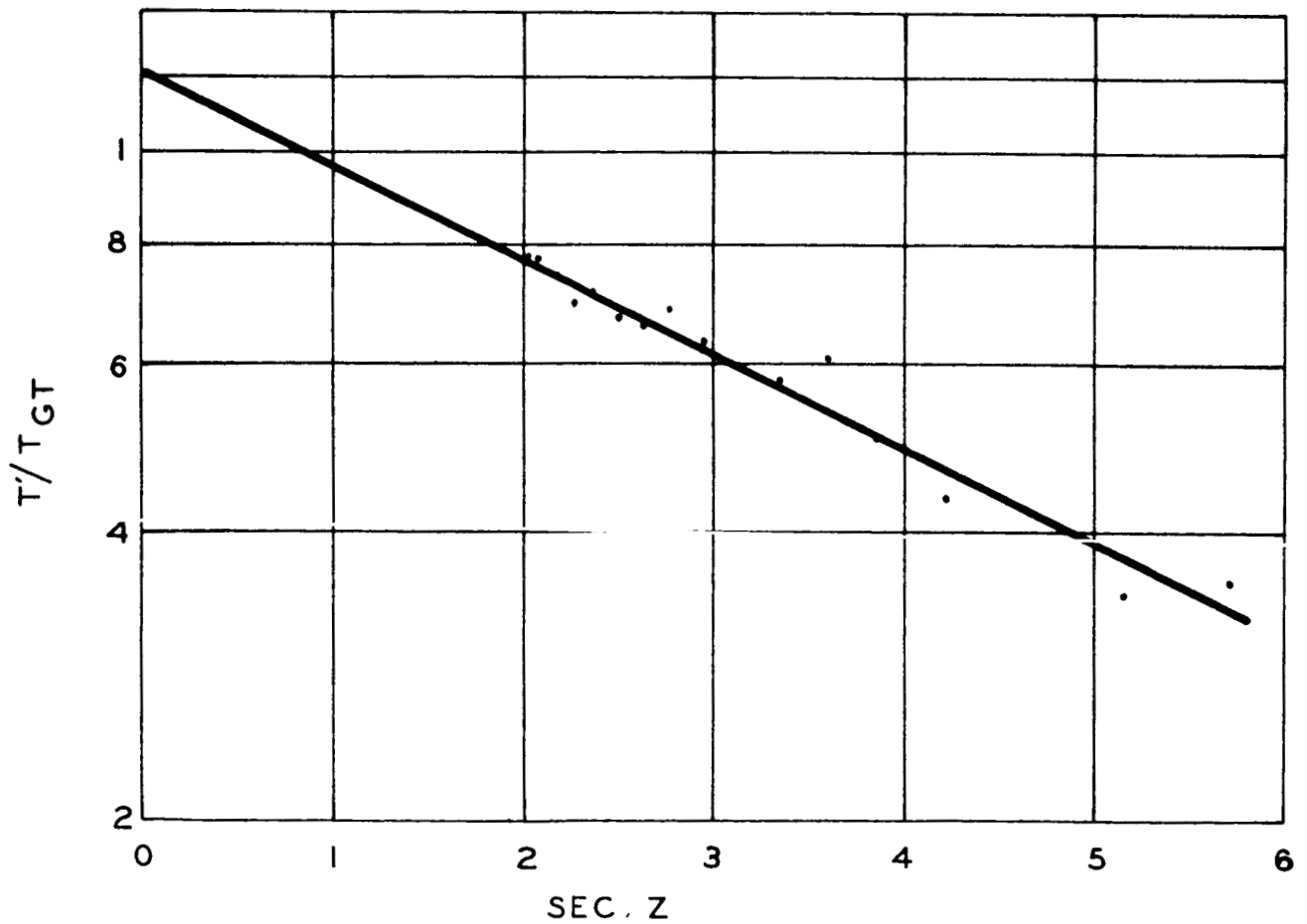
$$T'_M / T_{GT} = 1.197 \pm .048 \text{ (p. e.)}$$

$$L_0 = 1.248 \pm .042 \text{ (p. e.)}$$

Using $T_{GT} = 124.5$ and $BCF = .4916$ yields the equivalent blackbody disc temperature of the moon to be 303.1°K .

3. 19 December 1964 (6:28 - 8:13 PM PST)

16 drift curves were made on 19 December between 6:28 PM PST and 8:13 PM PST. The range of zenith angles was 79.9 to 60.0 deg. The data are presented in Fig. IV-6:



19-December-1964 Lunar Data (1800 - 2000 HR PST) with "Best-fit" Straight Line Approximation;

$$T'_M/T_{GT} = 1.225 \pm .032 \text{ (p. e.)}; L_0 = 1.255 \pm .011 \text{ (p. e.)}$$

Figure IV-6

The data yielded:

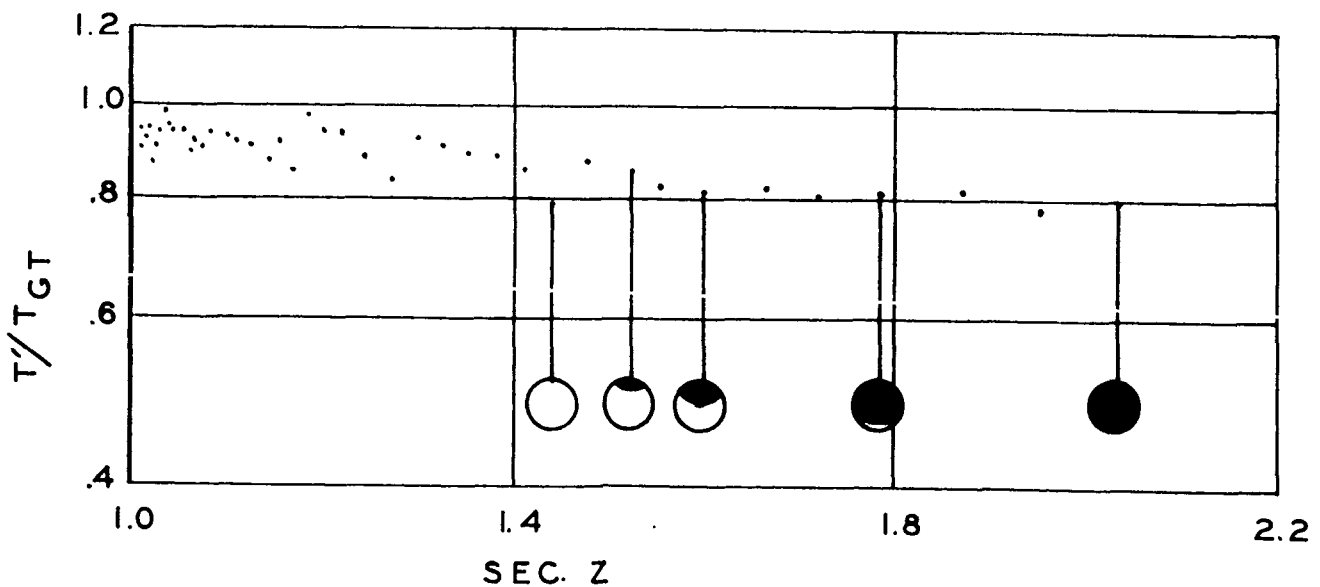
$$T'_M / T_{GT} = 1.225 \pm .032 \text{ (p. e.)}$$

$$L_0 = 1.255 \pm .011 \text{ (p. e.)}$$

and the corresponding blackbody disc temperature was 310.2°K .

4. 18 December 1964

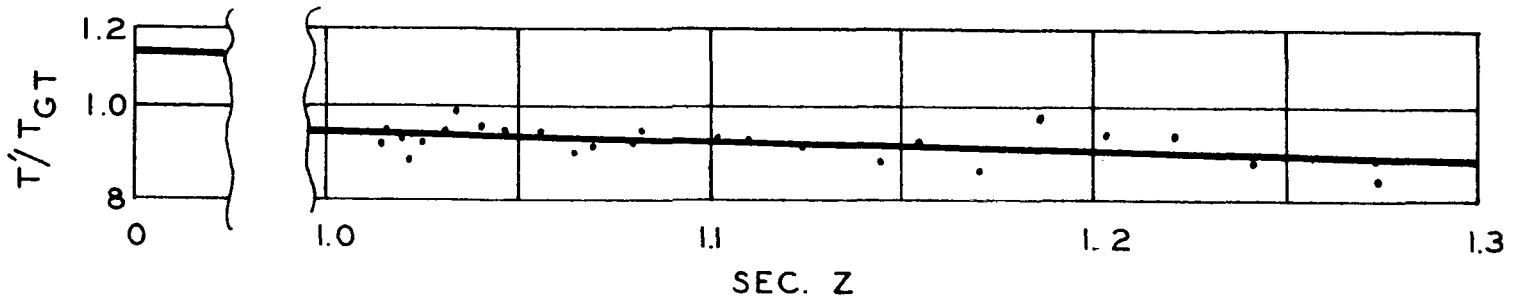
42 drift curves were made on 18 December between 7:10 PM PST and 11:53 PM PST. The first 11 drift curves, taken from 7:10 PM to 8:23 PM were made during the final umbral stages of the eclipse. The 42 data points are plotted in Fig. IV-7:



18-December-1964 Lunar Data During Final Stages of Total Lunar Eclipse

Figure IV-7

The final 26 data points, collected during the period from 9:02 PM to 11:53 PM, are plotted in Fig. IV-8:



18-December-1964 Lunar Data with "Best-fit" Straight Line Approximation;
 $T'_M/T_{GT} = 1.145 \pm .079$ (p. e.); $L_0 = 1.221 \pm .076$ (p. e.)

Figure IV-8

The moon left the penumbra at 9:14 PM. Assuming the 90-Gc thermal radiations from the moon had returned to equilibrium by 9:02, approximately two hours after the end of totality, the data in Fig. IV-8 yield:

$$T'_M/T_{GT} = 1.145 \pm .079 \text{ (p. e.)}$$

$$L_0 = 1.221 \pm .076 \text{ (p. e.)}$$

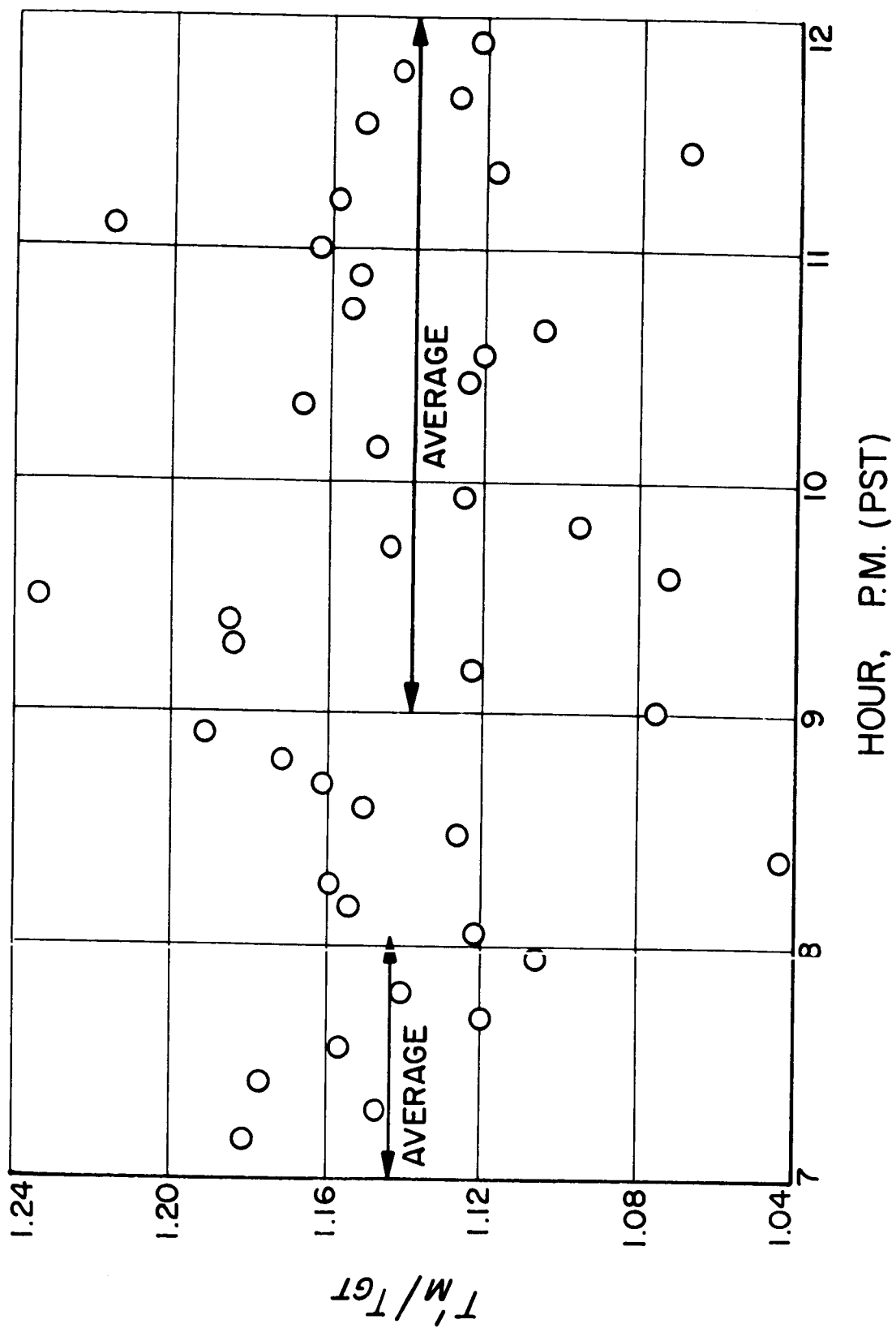
The corresponding value of the equivalent blackbody disc temperature is 290.0°K .

A final value for the average value of L_0 was obtained by reducing all of the 55 data points from 9:02 PM on 18 December to 3:54 AM on 19 December. These yield $L_0 = 1.215 \pm .034$ (p. e.). By multiplying each data point T'/T_{GT} of the 18-December data by a factor $L_0^{\text{sec } Z}$ it is possible to compute an equiv-

alent black-body disc antenna temperature ratio for the moon, T'_M/T_{GT} , for each point (cf. eq. IV-1). This has been done using $L_0 = 1.215$, and the results are plotted in Fig. IV-9. The average value of T'_M/T_{GT} for the 26 data points from 9:02 PM to 11:53 PM was $1.138 \pm .005$ (p. e.). The average value of T'_M/T_{GT} for the first 8 data points following the end of totality was $1.142 \pm .007$ (p. e.) and the average value for the 16 points between the end of totality and the end of the penumbral phase was $1.143 \pm .006$ (p. e.). The difference in average values of T'_M/T_{GT} for the 8 data points from 7:10 PM - 8:03 PM and for the 26 data points from 9:02 PM - 11:53 PM was $1.138 - 1.143 = -.005$.

Repeating this procedure using the best-fit value of L_0 minus one probable error (i. e. $1.215 - .034 = 1.181$) yields the average value of T'_M/T_{GT} for the 8 data points from 7:10 PM - 8:03 PM to be $1.086 \pm .005$ (p. e.) and the average value for the 26 data points from 9:02 PM - 11:53 PM to be $1.104 \pm .005$ (p. e.). The difference in average values is $1.104 - 1.086 = +.018$. The uncertainty in L_0 has caused an uncertainty in temperature change of $.018 - (-.005) = .023$. Consequently, the probable error in measurement of a temperature change in T'_M/T_{GT} is estimated to be $\sqrt{(.023)^2 + (.005)^2 + (.005)^2} = .024$. Converting this to moon temperature yields a probable error of 6.1°K . These results implicitly assume that L_0 remained constant during the observations.

The eclipse observations, therefore, as carried out with the 10.5-minute searchlight antenna beam, indicate no significant temperature difference between the data taken during the final umbral phase of the eclipse and the data taken 2-5 hours after the end of totality. The probable error of the measurement was estimated to be 6.1°K (moon temperature).



Lunar Equivalent Blackbody Disc Antenna Temperature Ratio vs. Time
 18 December 1964
 Figure IV - 9

B. Calculated Insolation Curve During Lunar Eclipse of 19 December

1964. A calculation* was made to determine the amount of solar radiation striking the surface of the moon during the eclipse. The important astronomical quantities are tabulated in Fig. IV-10. These quantities were used to determine the eclipse geometry as the moon entered and left the earth's shadow.

The amount of solar radiation present at any point within the penumbra of the earth's shadow was determined by geometrically finding the portion of the solar disc which was not occulted by the earth at that point, and then correcting for solar limb darkening. A small amount of solar radiation present within the umbra of the earth's shadow was due to refraction of the sun's rays by the earth's atmosphere. A refraction correction was included to account for the non-zero umbral intensity.

Figure IV-11 shows the amount of solar radiation striking the moon (as a function of time) for (1) a point at the center of the moon's disc, (2) for a central area with a diameter equal to 30% of the moon's diameter, and (3) for the entire surface of the moon.

C. One-Dimensional Heat-Flow Computer Program. In order to interpret the eclipse and lunation observations, a computer program was developed to calculate the expected lunar radiometric temperature as a function of solar insolation (lunation or eclipse), the thermal and electrical properties of the

* Complete details of this calculation may be found in "Eclipse Geometries and Lunar Brightness Curves for the Eclipses of December 30, 1963 and December 19, 1964", A. Cooper, Senior Thesis, Elect. Engineering Department, Univ. Southern California, June, 1965.

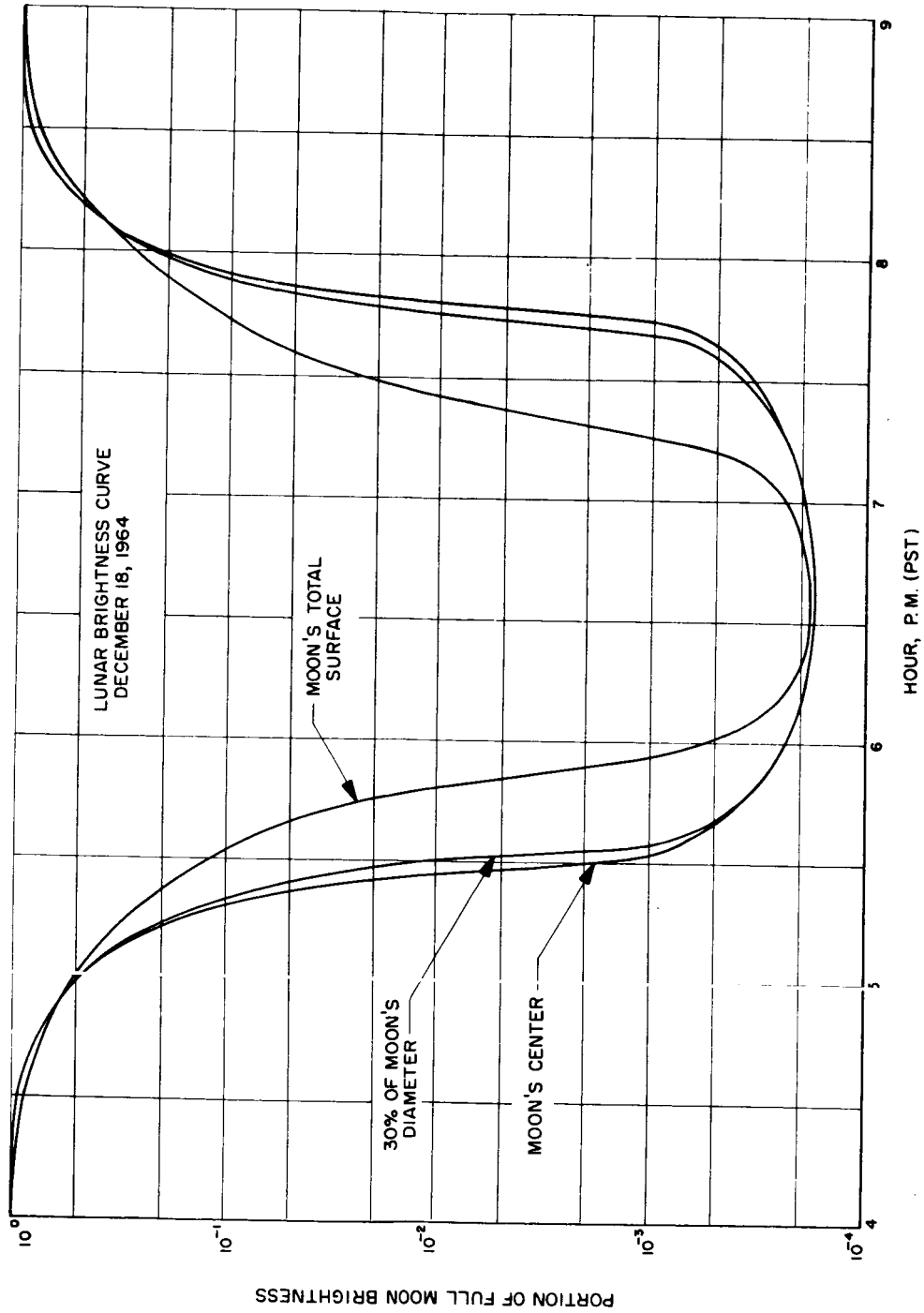
Ephemeris Time of Opposition in Right Ascension
December 19d 02h 42m 34.60s, 1964

Pacific Standard Time of Opposition in Right Ascension
December 18d 18h 41m 59.60s, 1964

R. A. of Sun	17h 47m 57.409s
R. A. of Shadow	5h 47m 57.409s
R. A. of Moon	5h 47m 57.409s
Decl. of Sun	- 23° 24' 54.34"
Decl. of Shadow	+ 23° 24' 54.34"
Decl. of Moon	+ 23° 48' 24.55"
Hourly Motion in R. A. of Sun	11.089s
Hourly Motion in R. A. of Shadow	11.089s
Hourly Motion in R. A. of Moon	166.107s
Hourly Motion in Decl. of Sun	- 0' 03.19"
Hourly Motion in Decl. of Shadow	+ 0' 03.19"
Hourly Motion in Decl. of Moon	+ 4' 19.01"
True Semidiameter of Sun	16' 15.4"
True Semidiameter of Moon	16' 44.3"
Equatorial Hor. Parallax of Sun	0' 08.94"
Equatorial Hor. Parallax of Moon	61' 25.92"
Ecliptic Longitude of Shadow	87.23722°
Ecliptic Longitude of Moon	87.24541°
Ecliptic Latitude of Moon	+ 0.39170°
Hourly Motion in Ecliptic Longitude of Moon Relative to Shadow	0.59269°
Hourly Motion in Ecliptic Latitude of Moon	+ 0.07107°
Geometrical Semidiameter of Umbra	0.75540°
Geometrical Semidiameter of Penumbra	1.29730°
Corrected Semidiameter of Umbra	0.77051°
Corrected Semidiameter of Penumbra	1.32325°
Moon Enters Penumbra	December 18d 04h 00.7m P. M. P. S. T.
Moon Enters Umbra	" " 04h 59.2m " "
Totality Begins	" " 06h 07.2m " "
Mid-Eclipse	" " 06h 37.3m " "
Totality Ends	" " 07h 07.3m " "
Moon Leaves Umbra	" " 08h 15.4m " "
Moon Leaves Penumbra	" " 09h 13.8m " "

Astronomical Parameters for the Total Lunar Eclipse
of December 19, 1964

Fig. IV-10



Solar Radiation Striking the Moon during the Lunar Eclipse of 19 December 1964
Figure IV-11

lunar surface, and their possible variation with depth. The one-dimensional heat-flow equations were numerically integrated after the method of Wesselink.* The basic heat-flow equation for a homogeneous one-dimensional layer is:

$$\frac{\partial^2 T(x, t)}{\partial x^2} = \frac{c\rho}{k} \frac{\partial T(x, t)}{\partial t} \quad (\text{IV-3})$$

where $T(x, t)$ = temperature, $^{\circ}\text{K}$; x = depth below surface, cm; t = time, sec; c = heat capacity, $\text{cal}/^{\circ}\text{K gm}$; ρ = density, gm/cm^3 ; k = thermal conductivity, $\text{cal}/^{\circ}\text{K cm sec}$. The nonlinear boundary condition at the surface ($x = 0$) is

$$\sigma e T^4(0, t) + \sqrt{k\rho c} \sqrt{\frac{k}{\rho c}} \frac{\partial T(0, t)}{\partial x} = (1 - A) I\left(\frac{t}{T_M}\right) \quad (\text{IV-4})$$

where $I\left(\frac{t}{T_M}\right)$ = solar energy flux impinging on the surface of the moon, $\text{cal}/\text{sec cm}^2$; σ = Stephan-Boltzmann constant, $1.37 \times 10^{-12} \text{ cal}/\text{cm}^2 \text{ sec } ^{\circ}\text{K}^4$; e = emissivity of the lunar surface; A = heat-balance albedo of the surface; and $\sqrt{k\rho c}$ = thermal inertia, $\text{cal}/^{\circ}\text{K cm}^2 \text{ sec}^{\frac{1}{2}}$. [The quantity $\gamma = (k\rho c)^{-\frac{1}{2}}$ is frequently used in the literature.] T_M = lunar month, $2.55 \times 10^6 \text{ sec}$.

Numerical integration of eqs. (IV-3) and (IV-4) yields $T(0, t)$ as a unique function of σe , $(1 - A)I\left(\frac{t}{T_M}\right)$, and $\sqrt{k\rho c}$. The solutions also yield temperature profiles as a function of the normalized depth parameter $z = \sqrt{\frac{\pi\rho c}{kT_M}} x$. To specify temperature profiles as a function of the absolute depth, x , in cm, it

* Wesselink, A. J., "Heat Conductivity and the Nature of the Lunar Surface Material", Bulletin of the Astronomical Institute of the Netherlands, April 23, 1948, Vol. 10, No. 390, p. 351.

is necessary to specify $\sqrt{\frac{k}{\rho c}}$ as well as $\sqrt{k\rho c}$.

The program initially computes temperature profiles (with depth) during a lunation. The temperature profiles may then be used to compute the radiometric temperature observed during the lunation. The radiometric temperature for a narrow-beam antenna directed normal to the surface is

$$T_{\text{RAD}}(f, t) = e_{\text{RAD}} \alpha_f \int_0^{\infty} T(x, t) e^{-\alpha_f x} dx \quad (\text{IV-5})$$

where e_{RAD} = radiometric emissivity and α_f = power attenuation constant, cm^{-1} . In db/cm α_f is 4.343 times its value in neper/cm . As a result of eq. (IV-5) the radiometric temperature is specified for given values of $\sqrt{k\rho c}$ and $\alpha_f \sqrt{\frac{k}{\rho c}}$, or, more simply, given values of $\sqrt{k\rho c}$ and $\alpha_f k$.

The lunation calculation is carried out using an iteration procedure until the temperature profile at the beginning of the lunation is consistent with the profile at the end of the lunation. The eclipse calculations use lunation profiles as the initial condition $T(x, 0)$.

D. Theoretical Radiometric Eclipse Curves for the Lunar Eclipse of 19 December 1964. The one-dimensional heat-flow program (Sec. IV-C) has been used in conjunction with the insolation curve of Fig. IV-11 to compute theoretical curves of radiometric temperature during the eclipse. Assuming that:

$$\begin{aligned} (k\rho c)^{\frac{1}{2}} &= 10^{-3} \\ \sigma e &= 1.3 \times 10^{-12} \end{aligned}$$

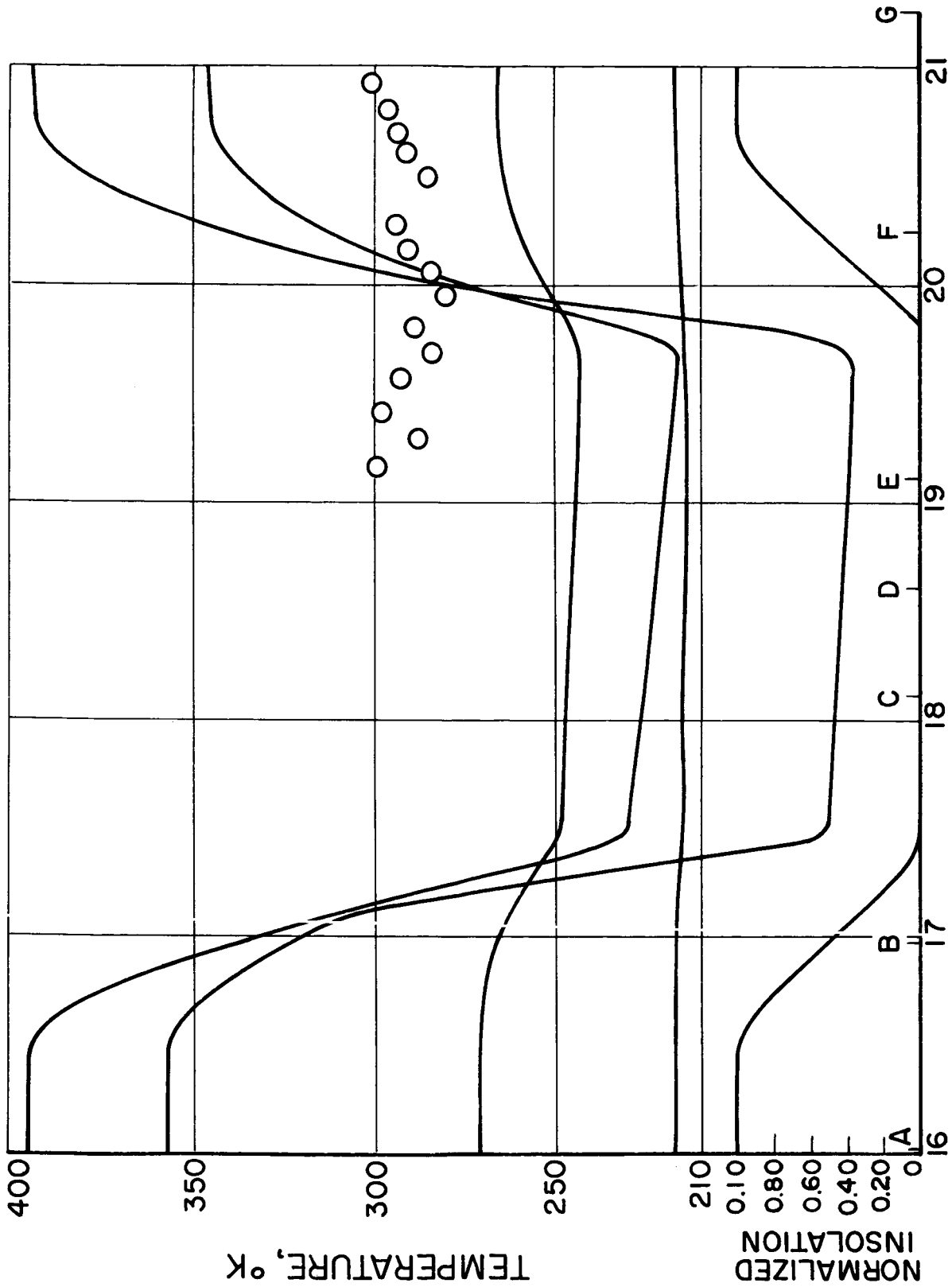
$$(1 - A) \times (\text{Solar Flux}) = 0.03167$$

$$e_{\text{RAD}} = 0.95$$

four curves of $T_{\text{RAD}}(f, t)$ vs. time were computed and are plotted in Fig. IV-12 for $\alpha_f \sqrt{\frac{k}{\rho c}} = \infty$ (curve 1); 10^{-2} (curve 2); 10^{-3} (curve 3); 10^{-4} (curve 4). The normalized insolation function at the center of the lunar disc is plotted at the bottom of Fig. IV-12. The time scale is local Pacific Standard Time on 18 December 1964. Also indicated along the abscissa axis are (A) moon enters penumbra; (B) moon enters umbra; (C) totality begins; (D) mideclipse; (E) totality ends; (F) moon leaves umbra; (G) moon leaves penumbra. The temperature decrease, ΔT , for curves (1), (2), (3), and (4) respectively are: 226°K ; 140°K ; 28°K ; and 3°K . In general, the initial temperature, the final temperature, and ΔT all increase as $\alpha_f \sqrt{\frac{k}{\rho c}}$ increases.

The data points from Fig. IV-9 have been converted into equivalent lunar disc temperature and are plotted on Fig. IV-12. It is not possible to reconcile these data points with any of the family of curves because the final temperature (288°K) is too high for a relatively small value of ΔT . It will be recalled from Sec. III-A that the measured temperature change was 0°K with a probable error of 6.1°K (i. e. $3\sigma = 27.1^{\circ}\text{K}$). Changing σe , $(1 - A) \times (\text{Solar Flux})$, and e_{RAD} over moderate ranges from the values assumed above will also not reconcile the 90-Gc radiometric data with the theoretical curves. Increasing $(k\rho c)^{\frac{1}{2}}$ from .001 to .0025 causes closer but not complete agreement.

Effects which have not been included in the calculations are (1) change in the solar insolation due to a normal lunation change over a period of 4 - 5



HOUR, P.M. (PST)

Comparison of Theoretical Radiometric Eclipse Curves and Observational Data
18 December 1964

Figure IV-12

hours; (2) variation of the angle of incidence over the antenna beam which will modify eq. (IV-5); (3) inhomogeneity of the thermal and electrical parameters along the surface or into the surface (e. g. more than one homogeneous layer); (4) antenna-beam averaging over different temperature contours on the lunar surface. The effects of (1) should cause temperature changes of less than a degree/hour. (2) - (4) are significant first-order effects and must be evaluated to allow further interpretation of the observational data. Final interpretation must also be consistent with lunation results.

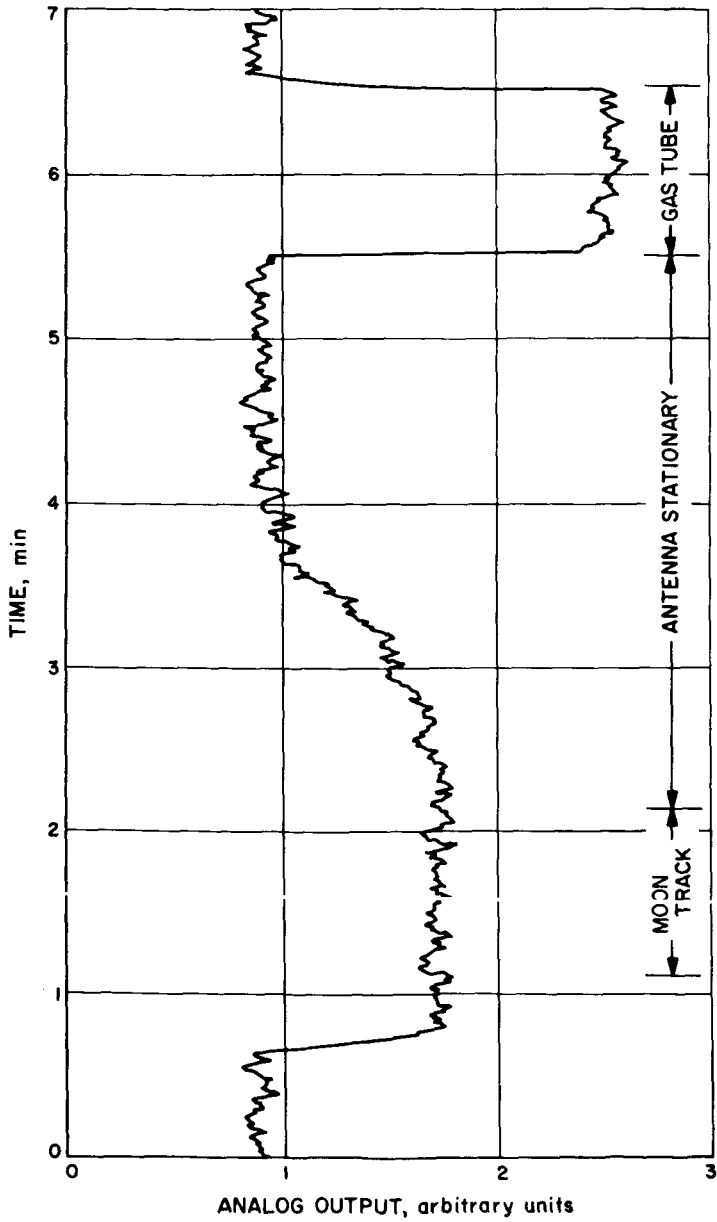
Systematic error in absolute thermal calibration of the radiometer (estimated to be 7 - 9% in Sec. V) would affect the absolute level of the equivalent lunar disc temperature but not the percentage change during the eclipse.

V. LUNATION OBSERVATIONS

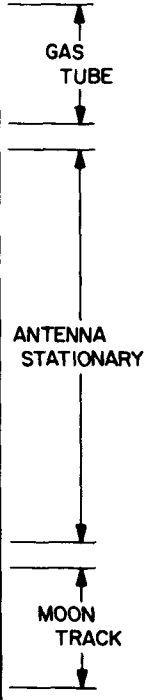
Radiometric observations of the sub-earth point on the moon were carried out daily during the period from 12 August 1965 to 12 September 1965. This period of time extended from a lunar phase of 190 deg, lunation 527, to a phase of 209 deg, lunation 528. These lunation observations, which yielded data of considerable scientific interest, also provided an excellent test for the long-term stability of the radiometer. Thermal calibration of the gas tube before and after each series of observations produced information on the long-term gas tube output. Another useful by-product of the observations was the data on atmospheric absorption.

A. Observations. The observational procedure closely followed the drift-curve procedure described in Section IV. Although an ambient termination was used as reference load in the Dicke system during the observations, several nights' data were obtained prior to 12 August using a wide-angle sky-horn as a relatively cool reference load. However, no significant improvement in sensitivity could be detected.

Two parallel systems were used to record the observational data: a Texas Instrument, Inc. strip-chart recorder, model FWD, driven from the radiometer with a one-second integrating time constant, and a Hewlett Packard, Inc. Digital Recorder 562A with an equivalent ten-second integrating time. The sample recordings plotted in Fig. V-1 are shown for drift-curve sequence #12 taken at a zenith angle of 65.05 deg on 10 August. Comparison with Fig. IV-3 showing a drift-curve sequence from the lunar eclipse $7\frac{1}{2}$ months earlier demonstrates the



TIME			OUTPUT								
2	2	1	1	5	8	4	1	8	7	1	1
2	2	1	1	4	5	4	2	4	1	4	1
2	2	1	1	3	3	4	2	7	0	2	1
2	2	1	1	2	1	6	8	5	9	7	1
2	2	1	1	0	8	6	8	5	7	0	1
2	2	1	0	5	6	6	9	2	4	6	1
2	2	1	0	4	3	6	8	1	1	2	1
2	2	1	0	3	1	6	8	1	2	2	1
2	2	1	0	1	9	4	2	8	3	1	1
2	2	1	0	0	6	4	2	4	9	1	1
2	2	0	9	5	4	4	2	6	1	6	1
2	2	0	9	4	9	4	2	8	2	6	1
2	2	0	9	2	9	4	2	3	8	0	1
2	2	0	9	1	4	4	2	6	0	5	1
2	2	0	9	0	4	4	2	6	9	8	1
2	2	0	8	5	2	4	3	3	6	8	1
2	2	0	8	7	6	4	4	2	6	8	1
2	2	0	8	2	7	4	6	5	1	9	1
2	2	0	8	1	4	4	9	4	5	0	1
2	2	0	8	0	2	5	1	9	9	0	1
2	2	0	7	5	0	5	2	8	4	8	1
2	2	0	7	3	7	5	5	1	1	5	1
2	2	0	7	2	5	5	4	8	5	3	1
2	2	0	7	1	2	5	6	2	9	2	1
2	2	0	7	0	0	5	6	1	6	3	1
2	2	0	6	4	8	5	6	0	2	2	1
2	2	0	6	3	5	5	5	9	6	9	1
2	2	0	6	2	3	5	5	5	2	1	1
2	2	0	6	1	7	5	5	7	3	7	1
2	2	0	5	5	8	5	6	3	7	1	1
2	2	0	5	4	5	5	6	1	6	3	1
2	2	0	5	3	3	4	5	3	9	3	1
2	2	0	5	2	1	4	3	1	4	5	1
2	2	0	5	0	8	4	2	2	8	5	1
2	2	0	4	5	6	4	2	8	6	8	1



Analog and Digital Recordings for Drift Curve #12
12 August 1965

Figure V-1

improved signal-to-noise ratio during the lunation (the amplitude of the gas-tube calibration is the same in both figures).

Frequent records of the temperature, pressure, and relative humidity were made during each series of observations.

A description of the raw data taken during the lunation observations is presented in Fig. V-2. The times are in Pacific Daylight Time. Observations on a particular date were made before meridian transit, after meridian transit, or both. The table presents the initial zenith angle and time, the final zenith angle and time, and the total number of drift curves of each series. Also recorded is the mean lunar phase at the mid-point of each day's observations (new moon is taken to be zero phase).

The gas-tube pulse was calibrated before and after each series. Several days of data were taken prior to 12 August but were not carefully calibrated and are not included. Noticable deterioration of the gas tube on 11 September and 12 September resulted in the data for these two days not being included in the final data reduction. A high statistical error on 21 August and 28 August caused the data for these two days to be discarded also.

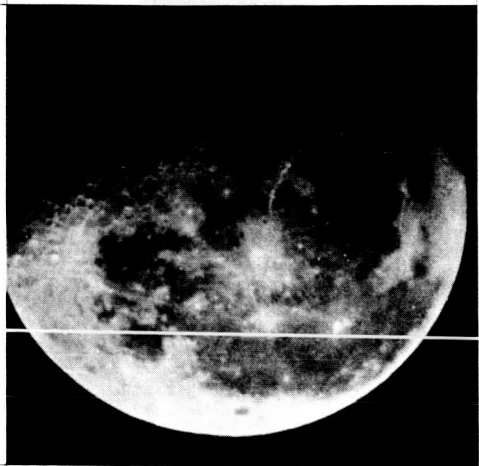
Photographs of the moon were taken with a phototheodolite concurrently with the radiometric observations. Samples of these are shown in Fig. V-3, showing the moon at various phases. Figure V-4 is a full-moon photograph (taken at Mt. Wilson) with a circle to indicate the half-power beamwidth of the antenna.

Date	Pre-transit				Post-transit				Phase deg					
	Pre-cal OK	Init. Z deg	Init. t _M	Final Z deg	Final t _M	No.	Mid-cal OK	Init. Z deg		Init. t _M	Final Z deg	Final t _M	No.	Post-cal OK
12 Aug	119.5	74.05	21:57:38	61.86	23:16:54	11	123.3							190
13 Aug	126.0	81.07	21:45:24	54.17	00:29:40 14 Aug	15	125.5							202
14 Aug	126.5	70.77	23:05:22	48.67	01:20:35 15 Aug	15	127.5							214
15 Aug	129.1	74.42	23:11:14	49.20	01:27:54 16 Aug	16	125.5							226
16 Aug	124.8	72.83	23:45:41	48.83	01:49:17 17 Aug	16	125.9							237
19 Aug	125.3	72.45	01:28:03 20 Aug	43.38	03:52:23 20 Aug	9	119.5	45.72	10:24:14 20 Aug	68.63	12:18:45 20 Aug	9	127.8	273
21 Aug							125.8	56.84	12:23:29	65.05	13:05:31	6	130.0	286
22 Aug							123.6	41.33	12:10:08	65.93	14:14:48	16	124.6	300
23 Aug	123.7	60.00	05:13:50	45.53	06:26:42	8								316
24 Aug	129.7	76.92	04:52:52	54.37	06:50:02	14	129.2							329
25 Aug	124.5	77.83	05:59:50	72.20	06:29:26	4								343
28 Aug							126.4	72.95	19:34:55	84.20	20:31:04	7		30
29 Aug							123.1	61.15	19:00:13	74.10	20:10:06	9		42
30 Aug							126.7	59.78	19:13:34	70.03	20:15:47	8	127.7	56
31 Aug								53.37	18:30:07	71.83	20:53:13	15	118.5	68
1 Sep							114.7	56.75	19:08:47	70.68	21:11:08	13	119.6	81
2 Sep	116.0	66.67	16:26:29	59.95	17:40:44	8		57.73	18:45:51	70.35	21:44:00	14		93
3 Sep	116.0	70.02	17:04:10	60.73	18:56:47	11		61.93	20:51:38	70.45	22:22:42	10	118.0	104
4 Sep	122.3	68.60	18:14:13	61.53	19:46:56	9		60.70	20:48:08	69.85	23:03:43	13	119.8	116
7 Sep	117.2	67.27	20:19:42	55.62	23:06:40	13		57.52	00:05:47 8 Sep	69.07	02:05:40 8 Sep	13	117.1	150
8 Sep	117.5	67.45	20:42:03	51.92	23:41:51	15		54.43	00:58:34 9 Sep	69.70	03:08:10 9 Sep	15	122.6	161
9 Sep	117.4	64.88	21:17:54	48.75	23:46:11	14		48.83	01:23:27 10 Sep	70.75	04:18:28 10 Sep	15	120.3	173
10 Sep	123.2	66.10	21:35:54	45.15	00:06:41 11 Sep	14		46.17	02:35:01 11 Sep	70.65	05:19:42 11 Sep	14	126.0	185
11 Sep	113.0	66.78	21:54:51	43.55	00:16:06 12 Sep	13		46.68	04:01:35 12 Sep	70.07	06:17:25 12 Sep	15	114.2	197
12 Sep	95.0	66.83	22:19:01	44.97	00:17:47 13 Sep	15		46.53	05:11:00 13 Sep	70.37	07:18:29 13 Sep	15	96.9	209

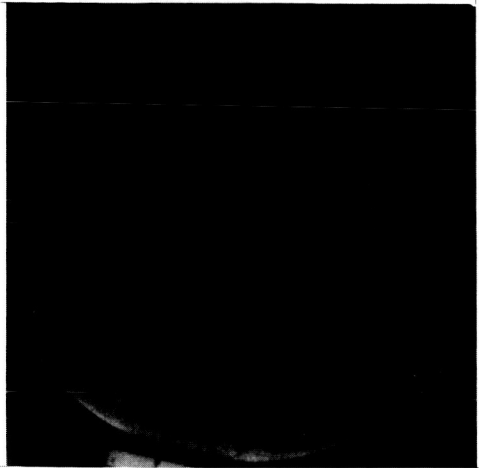
Tabulation of Data from Lunation Observations
Figure V-2



14 AUG. 1965
 $\phi_M = 214$ DEG.



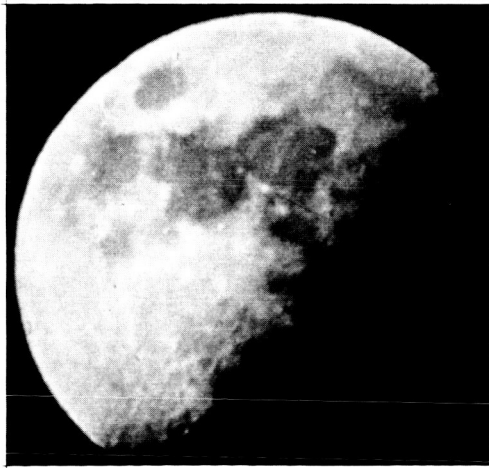
16 AUG. 1965
 $\phi_M = 237$ DEG.



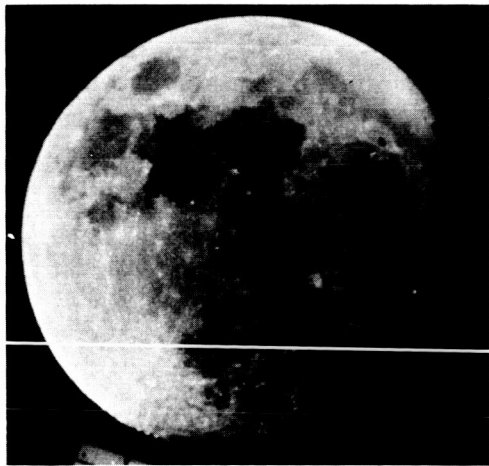
25 AUG. 1965
 $\phi_M = 343$ DEG.



2 SEPT. 1965
 $\phi_M = 93$ DEG.



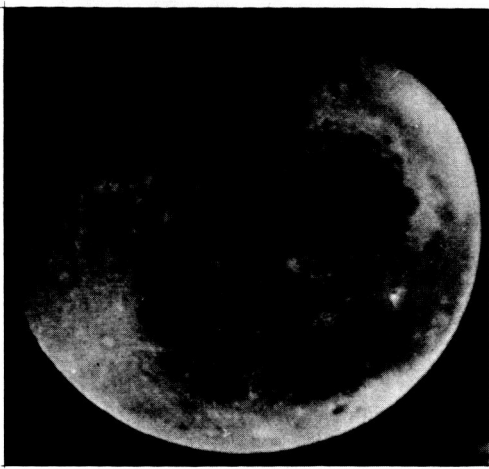
4 SEPT. 1965
 $\phi_M = 116$ DEG.



8 SEPT. 1965
 $\phi_M = 161$ DEG.



10 SEPT. 1965
 $\phi_M = 185$ DEG.



12 SEPT. 1965
 $\phi_M = 209$ DEG.

Sample Photos of Moon taken during Lunation

Figure V-3

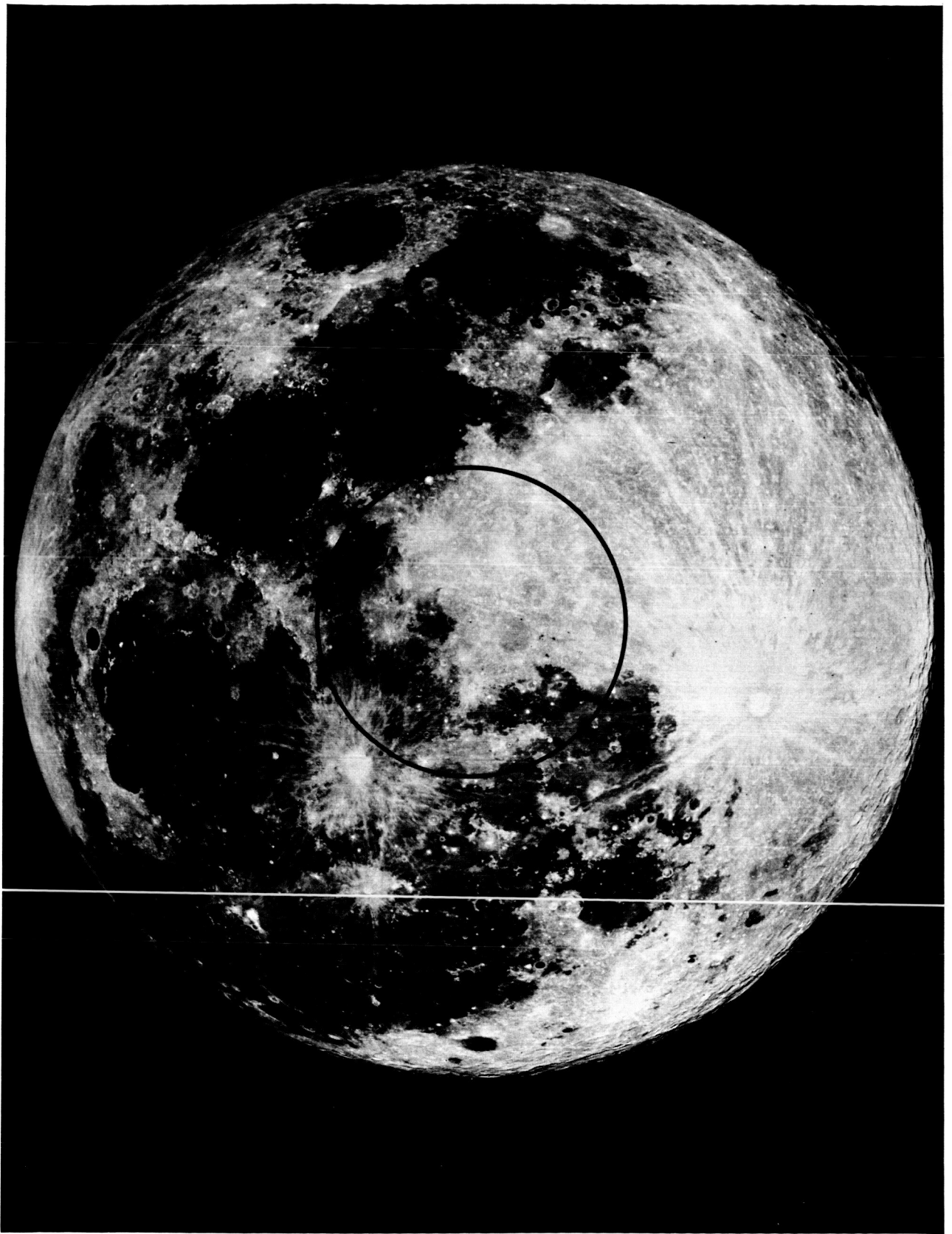


Photo of Moon with Relative Size of Half-Power Beamwidth

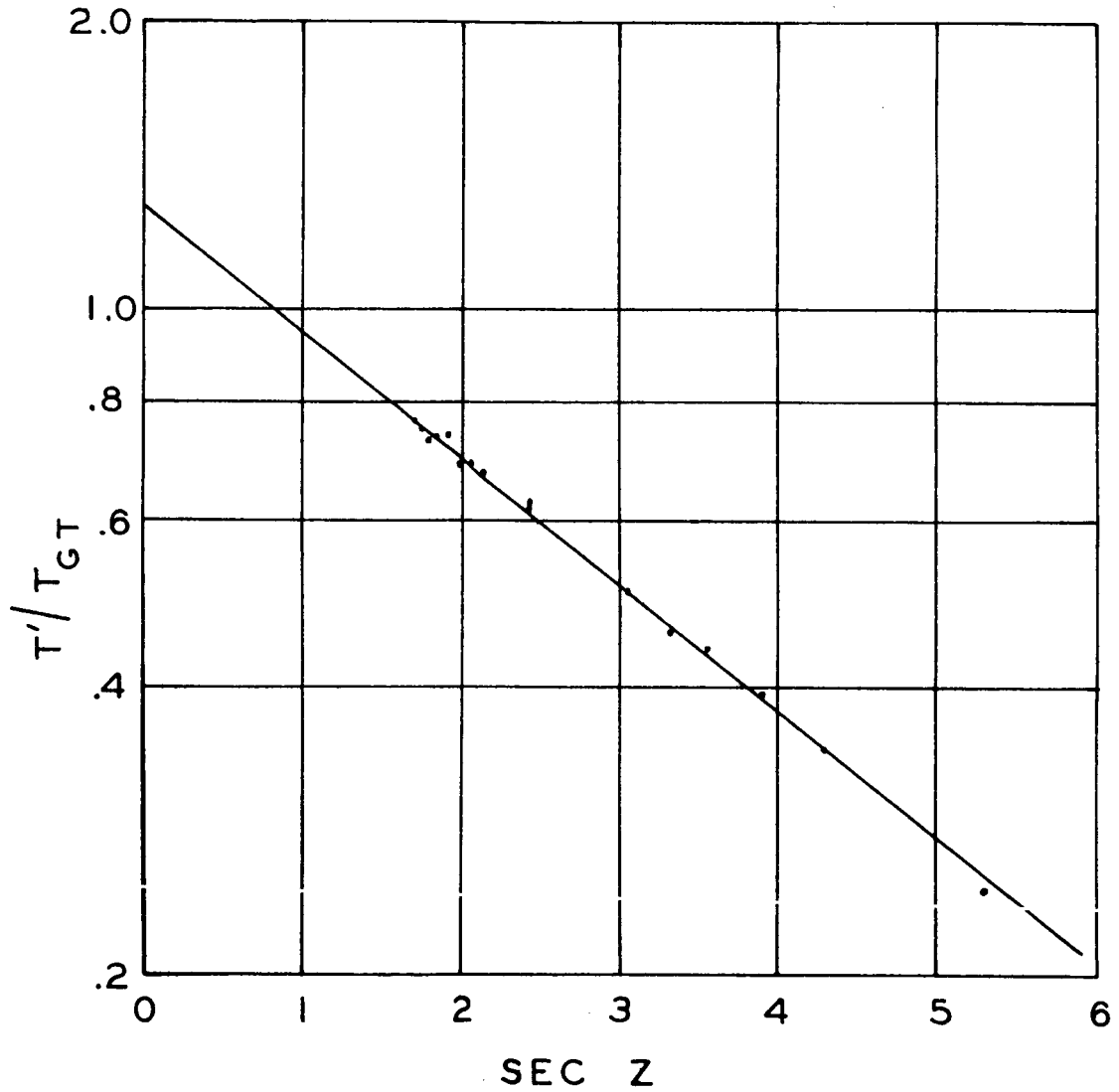
Figure V-4

B. Data Reduction. The least-squares-fit iteration procedure described in Section IV was used to evaluate the atmospheric absorption for each series of observations. It was thus possible to obtain an equivalent antenna temperature for the lunar disc for each series. A typical result is shown in Fig. V-5 for 13 August 1964. The observed temperature/gas tube ratio is plotted versus the secant of the observed zenith angle. The ratio of the equivalent lunar disc temperature/gas tube is 1.290 ± 0.012 (p. e.); the zenith atmospheric loss is 1.359 ± 0.005 (p. e.). These two values yield the straight line superimposed upon the data.

Repeating this procedure for each series of observations yields the results tabulated in Fig. V-6. The column headings are T'_M/T_{GT} , the ratio of the equivalent lunar antenna temperature to the equivalent gas-tube temperature at the output of the waveguide switch (with the statistical probable error), and the atmospheric loss at zenith (with the statistical probable error). Results are tabulated for both pre-transit and post-transit observations when available.

Gas-tube calibrations were carried out for each series of observations as indicated in Fig. V-2. These calibrations consisted of manually switching the waveguide switch between an ambient load, a hot load (at a temperature of approximately 125°C), and the gas tube. The gas-tube output passed through a 10-db calibrated attenuator and a 10-db directional coupler into the main rf path. The calibration reference point was the output of the waveguide switch.

The results of the calibrations are plotted in Fig. V-7. In addition to appreciable scatter of the data points there appeared to be a gradual decline in



13-August-1965 Lunar Data with "Best-fit" Straight Line Approximation; $T'_M/T_{GT} = 1.290 \pm .012$ (p. e.); $L_0 = 1.359 \pm .005$ (p. e.)

Figure V-5

Date	Pre-transit		Post-transit		Phase
	$T'_M/T_{GT} \pm \text{p.e.}$	Zen. Loss $\pm \text{p.e.}$	$T'_M/T_{GT} \pm \text{p.e.}$	Zen. Loss $\pm \text{p.e.}$	
12 Aug	1.114 .030	1.390 .014			190
13 Aug	1.290 .012	1.359 .005			202
14 Aug	1.172 .027	1.356 .015			214
15 Aug	1.143 .013	1.302 .007			226
16 Aug	1.201 .024	1.356 .013			237
19 Aug	.997 .036	1.237 .020	.887 .020	1.198 .014	273
21 Aug			.852 .105	1.172 .068	286
22 Aug			.853 .017	1.224 .014	300
23 Aug	.926 .062	1.281 .051			316
24 Aug	.814 .019	1.180 .011			329
25 Aug	.661 .050	1.065 .020			343
28 Aug			1.421 .320	1.437 .077	30
29 Aug			.659 .049	1.223 .034	42
30 Aug			.576 .022	1.118 .018	56
31 Aug			.629 .026	1.134 .021	68
1 Sep			.537 .022	1.069 .019	81
2 Sep	.424 .038	.989 .039	.615 .029	1.137 .024	93
3 Sep	.799 .034	1.201 .021	.691 .023	1.115 .015	104
4 Sep	.804 .062	1.407 .046	.617 .050	1.206 .042	116
7 Sep	1.009 .041	1.237 .024	.888 .024	1.129 .013	150
8 Sep	1.107 .019	1.224 .011	.989 .010	1.124 .005	161
9 Sep	.962 .014	1.123 .009	.991 .015	1.113 .008	173
10 Sep	1.164 .018	1.165 .010	1.112 .010	1.147 .005	185
11 Sep	1.165 .017	1.124 .009	1.174 .009	1.081 .004	197
12 Sep	1.542 .025	1.126 .010	1.458 .055	1.061 .020	209

Table of Equivalent Lunar Antenna Temperature Ratio and Atmospheric Loss for Lunation Observations

Figure V-6

the gas-tube output. The best-fit straight line approximation to the equivalent excess noise temperature of the gas tube through the 10-db attenuator and 10-db directional coupler was

$$T_{GT} (^{\circ}K) = 129.4 (\pm 1.4 \text{ p. e.}) - 0.26 (\pm 0.05) \times \text{Day Number} \quad (V-1)$$

The Day Number is the date in August or the date in September plus 31. The resulting gas-tube temperatures calculated from the above formula are tabulated in Fig. V-8. The probable error on each value is $2.4^{\circ}K$. Also tabulated is T'_M/T_{GT} , as it appeared in Fig. V-6. The data for 21 August and 28 August have been discarded because of excessively large values of probable error; the data for 11 September and 12 September have been discarded because of deterioration of the gas-tube output.

Multiplication of T'_M/T_{GT} by T_{GT} yields T'_M , the equivalent black-body lunar disc antenna temperature at the output of the waveguide switch. T'_M is defined:

$$T'_M = \left[\frac{G_A \ell}{4\pi} \int_{\text{moon}} f(\Omega) d\Omega \right] T_{MD} \quad (V-2)$$

where G_A = 90-Gc gain of 60-inch antenna in plane of aperture = 4.92×10^5
 ℓ = loss between antenna aperture and output of waveguide switch
 $f(\Omega)$ = normalized antenna pattern
 T_{MD} = equivalent black-body disc temperature of the moon.

Date	Pre-transit			Post-transit			Phase
	T_{GT}	$T_M \pm p.e.$	T_M/T_{GT}	T_{GT}	$T_M \pm p.e.$	T_M/T_{GT}	
12 Aug	126.3	140.7 4.6					190
13 Aug	126.1	162.6 3.4					202
14 Aug	125.8	147.4 4.4					214
15 Aug	125.6	143.5 3.2					226
16 Aug	125.3	150.5 4.2					237
19 Aug	124.5	124.1 5.1	.887 .020	124.5	110.4 3.3		273
22 Aug			.853 .017	123.7	105.5 3.3		300
23 Aug	123.5	114.3 7.9					316
24 Aug	123.2	100.3 3.0					329
25 Aug	123.0	81.3 6.3					343
29 Aug			.659 .049	121.9	80.3 6.1		42
30 Aug			.576 .022	121.6	70.1 4.0		56
31 Aug			.629 .026	121.4	76.3 3.4		68
1 Sep			.527 .022	121.1	65.0 2.9		81
2 Sep	120.9	51.2 4.7	.615 .029	120.9	74.3 3.8		93
3 Sep	120.6	96.4 4.5	.691 .023	120.6	83.3 3.2		104
4 Sep	120.3	96.7 7.7	.617 .050	120.3	74.2 6.2		116
7 Sep	119.6	120.6 5.4	.888 .024	119.6	106.2 3.6		150
8 Sep	119.3	132.1 3.4	.989 .010	119.3	118.0 2.7		161
9 Sep	119.0	114.5 2.6	.991 .015	119.0	118.0 3.0		173
10 Sep	118.8	138.2 3.6	1.112 .010	118.8	132.1 2.9		185

Table of Reduced Antenna Temperatures for Lunation Observations

Figure V-8

The pattern measurements described in Section IIID yielded

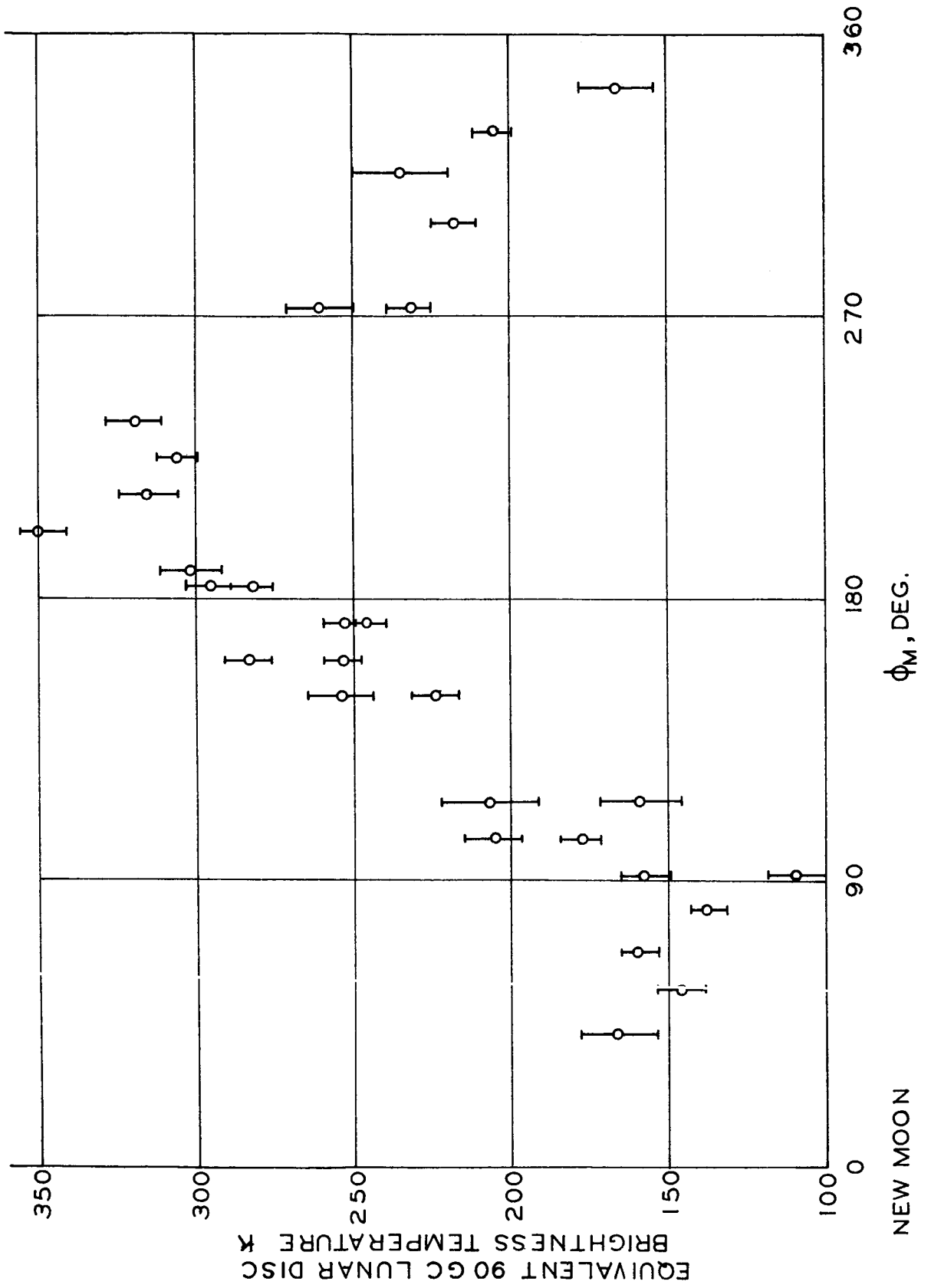
$$\int_{\text{moon}} f(\Omega) d\Omega = \begin{cases} 1.17 \times 10^{-5}, & \text{14-minute semi-diameter} \\ 1.20 \times 10^{-5}, & \text{15-minute semi-diameter} \\ 1.23 \times 10^{-5}, & \text{16-minute semi-diameter} \\ 1.26 \times 10^{-5}, & \text{17-minute semi-diameter} \end{cases} \quad (\text{V-3})$$

The bracketed expression in eq. (V-2), defined as the Beam-Correction-Factor or BCF, is

$$\text{BCF} = \frac{G_A / \ell}{4\pi} \int_{\text{moon}} f(\Omega) d\Omega = \begin{cases} .457, & \text{14-minute semi-diameter} \\ .470, & \text{15-minute semi-diameter} \\ .482, & \text{16-minute semi-diameter} \\ .495, & \text{17-minute semi-diameter} \end{cases} \quad (\text{V-4})$$

Thus a BCF may be obtained for each data point, corresponding to the angular semi-diameter of the moon on that date. During the observations the lunar semi-diameter ranged from approximately 14.7 min to 16.7 min.

Division of T'_M by the values of BCF yields T_{MD} , the equivalent black-body disc temperature of the moon. The resulting values of T_{MD} are plotted in Fig. V-9 as a function of lunar phase. In many cases the probable error flags, computed from the statistical scatter of the observations, do not overlap to produce a smooth curve. This effect is attributed to temporal variations in the atmospheric absorption during a series of observations. Such temporal variations can cause significant errors in the zero-atmosphere extrapolated



Equivalent Lunar Blackbody Disc Temperature vs. Phase

Figure V-9

intercept value of T'_M/T_{GT} .¹

In addition to the statistical measurement errors, errors were also introduced in the determination of the BCF values and in the thermal calibration of the gas tube. Such errors will produce an uncertainty in the ordinate scale factor in Fig. V-9. This uncertainty is estimated to be 7-9%, primarily due to the gain-measurement uncertainty of 0.25 db.

The values of T_{MD} have been fitted with the first two terms of a Fourier series:

$$T_{MD} = T_0 - T_1 \cos(\phi_M - \theta) \quad (V-5)$$

Weighting factors inversely proportional to the square of the probable error of each data point were used. The results of this calculation were:

$$T_0 = 215.8 \text{ } ^\circ\text{K} \pm 3.4 \text{ } ^\circ\text{K (p. e.)}$$

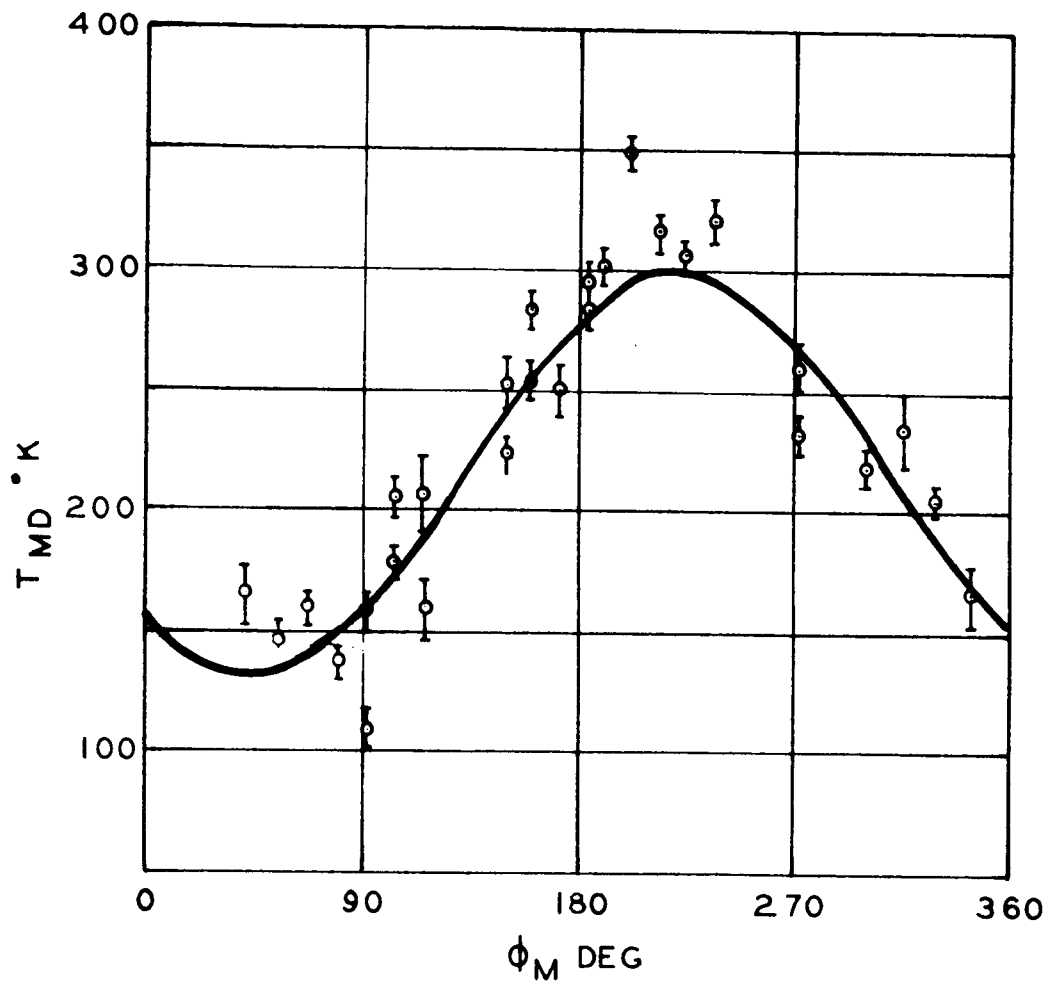
$$T_1 = 85.1 \text{ } ^\circ\text{K} \pm 4.5 \text{ } ^\circ\text{K (p. e.)}$$

$$\theta = 42.3 \text{ deg} \pm 1.8 \text{ deg (p. e.)}$$

The resulting best-fit curve is plotted in Fig. V-10 with the original data points. The probable error computed from deviations from the curve is 15.7 $^\circ\text{K}$. The radiometric maximum lags full-moon by a significant part of a lunar period.

The lunar heat-flow program described in Section IV may be used to

¹ F.I. Shimabukuro, "Propagation Through the Atmosphere at a Wavelength of 3.3 mm". SSD-TR-65-69, Aerospace Corp., El Segundo, Calif.



Best-fit Cosine Superimposed on Lunation Results

Figure V-10

compute the expected radiometric temperature of a one-dimensional model of the moon. A typical result is superimposed on the data in Fig. V-11. The assumed parameters for the computed curve are:

$$(k\rho c)^{\frac{1}{2}} = 10^{-3}$$

$$\sigma e = 1.3 \times 10^{-12}$$

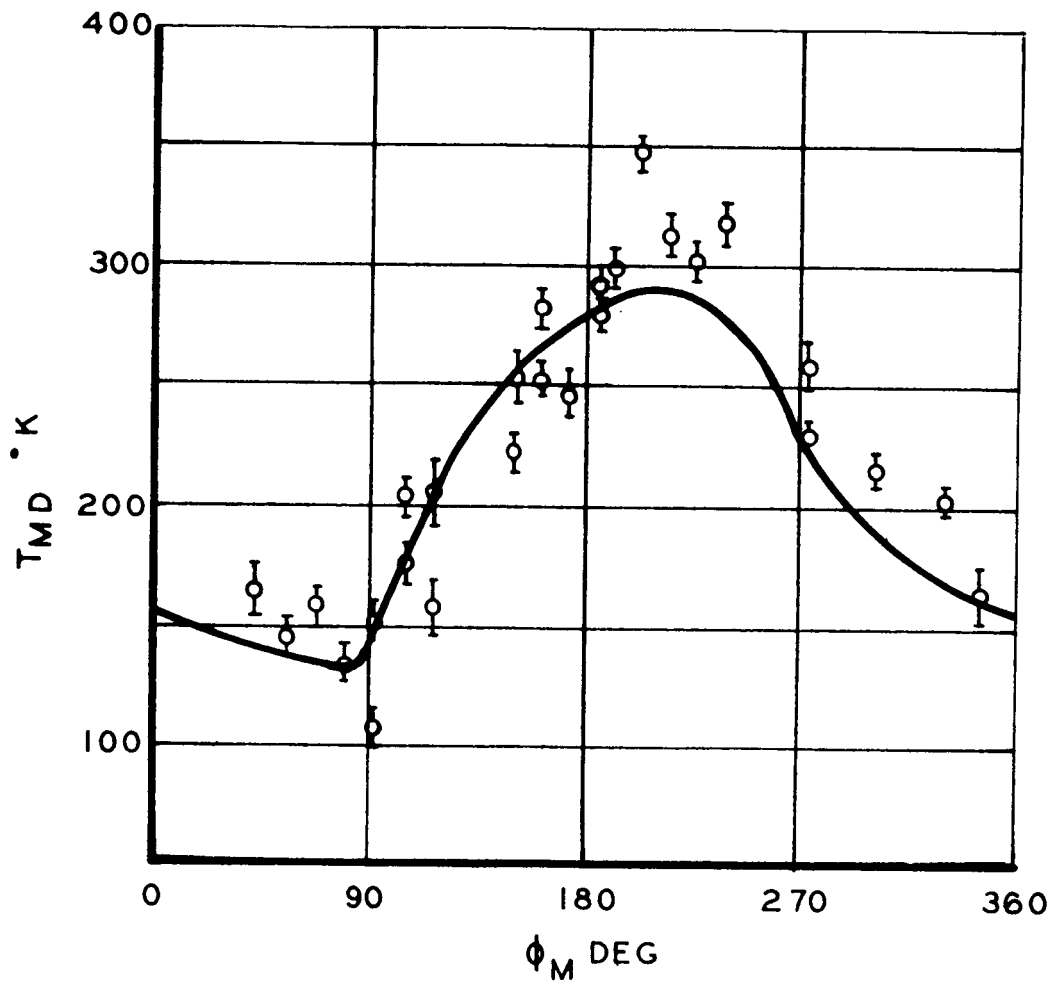
$$(1-A) \times (\text{Solar Flux}) = 0.03167$$

$$e_{\text{RAD}} = 0.95$$

$$\text{thermal conductivity, } k, = 2.5 \times 10^{-6} \text{ cal/}^{\circ}\text{K cm sec}$$

$$\begin{aligned} \text{power attenuation constant of a single-layered model} \\ = 2.2 \text{ db/cm} \end{aligned}$$

The resulting probable error based on the scatter of the experimental points about the computed curve is 18.1 °K. The experimental points do not justify attempts at further refinements of the above values. However, unless the power attenuation constant of a single-layered model is of the order of magnitude of the value shown above, it is not possible to match the peak-to-peak temperature variation of 150 °K and phase lag of 20 - 40 deg using "conventional" values for the other thermal and electrical parameters of a one-dimensional model.



Theoretical Lutation Curve with Observational Results

Figure V-11

ACKNOWLEDGEMENT

We wish to acknowledge several individuals who have participated in this program. Mr. Robert Gardner of JPL was primarily responsible for radiometer development and trouble-shooting (at any hour of the day or night). Without his services this program would not have been possible. Mr. M. Reid and Mr. K. Wallace of JPL, and Mr. R. Adams, Mr. R. Connett, Mr. A. Cooper, and Mr. M. Dooley of USC assisted with the observing. Mr. L. Holmes assisted with the lunation calculations and Mr. P. Poulson developed the computer program. Mr. A. Cooper carried out the calculation of the insolation function during the eclipse. Finally, we wish to acknowledge the encouragement of Dr. W. Higa and Mr. R. Stevens of JPL who were responsible for the initial funding of the program.

5 APR 66 36838

USG *Engineering*